AD-A069 024 LITTON SYSTEMS INC WOODLAND HILLS CA GUIDANCE AND CO--ETC F/G 17/7
NUCLEAR MOMENT ALIGNMENT, RELAXATION AND DETECTION MECHANISMS.(U)
MAR 79 C H VOLK F49620-77-C-0047
UNCLASSIFIED G/CSD-TR-404312 AFOSR-TR-79-0599 NL

1 OF 1
AD A069024

END
DATE FILMED
7-79
DDC

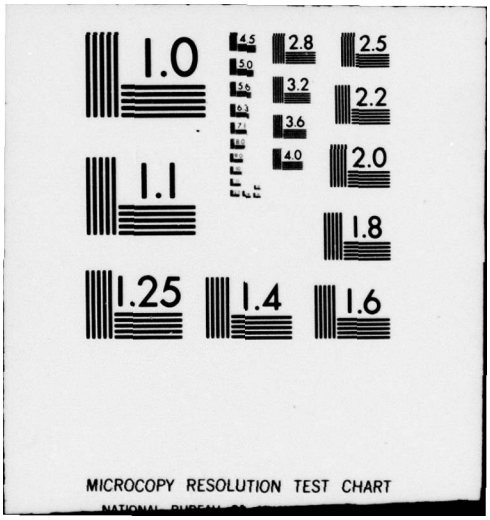
1.0
1.1
1.25
1.4
1.6
1.8
2.0
2.2
2.5
2.8
3.2
3.6
4.0
4.5
5.0
5.6
6.3
7.1
8.0
9.0
MICROCOPY RESOLUTION TEST CHART

Document No. 404312

LEVEL II (3)

AFOSR-TR. 79-0599

NUCLEAR MOMENT ALIGNMENT, RELAXATION AND DETECTION MECHANISMS

February 1978 – January 1979

ANNUAL TECHNICAL REPORT

Contract No. F49620-77-C-0047

Prepared for

AIR FORCE OFFICE OF SCIENTIFIC RESEARCH

Litton GUIDANCE & CONTROL SYSTEMS
5500 Canoga Avenue, Woodland Hills, California 91365

UNCLASSIFIED

SECURITY CLASSIFICATION OF THIS PAGE (When Data Entered)

REPORT DOCUMENTATION PAGE	READ INSTRUCTIONS BEFORE COMPLETING FORM
1. REPORT NUMBER: AFOSR-TR-79-0599	2. GOVT ACCESSION NO. / 3. RECIPIENT'S CATALOG NUMBER
4. TITLE (and Subtitle): NUCLEAR MOMENT ALIGNMENT, RELAXATION AND DETECTION MECHANISMS	5. TYPE OF REPORT & PERIOD COVERED: Interim (February 1978–January 1979)
	6. PERFORMING ORG. REPORT NUMBER: 404312
7. AUTHOR(s): C. H. Volk	8. CONTRACT OR GRANT NUMBER(s): F49620-77-C-0047
9. PERFORMING ORGANIZATION NAME AND ADDRESS: Litton, Guidance & Control Systems Div. 5500 Canoga Ave. Woodland Hills, CA. 91365	10. PROGRAM ELEMENT, PROJECT, TASK AREA & WORK UNIT NUMBERS
11. CONTROLLING OFFICE NAME AND ADDRESS: Director of Physics Code FQ 8671, Air Force Office of Scientific Research, Attn: NP Building 410, Bolling AFB, D.C. 20332	12. REPORT DATE: Mar 1979 / 13. NUMBER OF PAGES: 66 (68p.)
14. MONITORING AGENCY NAME & ADDRESS (if different from Controlling Office): Same	15. SECURITY CLASS. (of this report): UNCLASSIFIED
Charles H. Volk	15a. DECLASSIFICATION/DOWNGRADING SCHEDULE

16. DISTRIBUTION STATEMENT (of this Report)

Approved for public release; distribution unlimited.

Annual technical rept. Feb 78 - Jan 79

17. DISTRIBUTION STATEMENT (of the abstract entered in Block 20, if different from Report)

G/CSD-TR-404312

18. SUPPLEMENTARY NOTES

19. KEY WORDS (Continue on reverse side if necessary and identify by block number)

Nuclear Magnetic Resonance	Nuclear Moment Relaxation
Gyroscope	Quadrupole Relaxation
Optical Pumping	Nuclear Moment Precession
Nuclear Moment Alignment	Spin Exchange

20. ABSTRACT (Continue on reverse side if necessary and identify by block number)

The reported physics research is part of an overall program to develop a nuclear magnetic resonance gyro that makes use of an optically pumped alkali metal vapor both to align the magnetic moments of noble gas nuclei and to detect the weak magnetic fields that are generated by the precession of these nuclear moments.

A model for the role of the alkali-atom-noble-gas-atom Van der Waals molecule in the alkali electronic, noble gas nuclear spin exchange process has been developed. It has been found that

next page

DD FORM 1473 EDITION OF 1 NOV 65 IS OBSOLETE

20. ABSTRACT (continued)

spin exchange in the presence of the molecular formation is significantly more efficient than that for simple fly–by collisions. Preliminary experimental results have verified the general features of the molecular model.

The theory for the quadrupole relaxation of noble gas nuclei in wall collisions has been developed. Experimental studies of krypton nuclear relaxation revealed a decay mode which was a function of the angular orientation of the cell in the apparatus and which was found to lead to a non–exponential type of decay signal. The model of the noble gas quadrupolar relaxation was found to explain all observations in the krypton experiments.

TABLE OF CONTENTS

TABLE OF CONTENTS (cont)

SECTION I

PROGRAM DESCRIPTION

1.1 INTRODUCTION

Litton's Guidance and Control Systems Division is involved in a multi-year program in the research and development of a nuclear magnetic resonance (NMR) gyro for use in inertial navigation systems.

Angular rate is sensed in an NMR gyro through a shift in the Larmor frequency of an ensemble of precessing atomic or nuclear magnetic moments. In the Litton approach, two different noble gas nuclear isotopes are used to eliminate explicit dependence on the magnetic field. The noble gas ensembles attain a net magnetic moment through spin exchange collisions with an optically oriented alkali metal vapor. In addition, the alkali vapor, through a magnetometer effect, detects the weak magnetic fields which are generated by the precessing nuclear moments of the two noble gases, and thus provides the gyro angular rate information.

The aim of the physics research program reported here, is to develop a stronger theoretical and empirical understanding of the alkali-atom-noble-gas nuclear spin exchange process, noble gas spin relaxation mechanisms and other related NMR phenomena in a noble-gas-alkali-metal vapor system.

Results of the studies will be relevant not only to the development of an NMR gyro but also in improving the basic understanding of noble gas alkali atomic interactions and will therefore be of interest to many investigators in related fields.

1.2 OBJECTIVES AND STATUS OF THE CURRENT PROGRAM

The research tasks described in Sections II and III are aimed at providing a better understanding of spin dynamic properties of a polarized noble gas nuclear ensemble in a noble gas, alkali metal vapor system. Investigations into this area of atomic physics have relevance not only to NMR gyro research, but also to other possible areas of research such as maser, magnetometers and polarized nuclear targets.

In Section II a theory for the role of the alkali atom, noble gas atom, Van der Waals molecules in the alkali electronic noble gas nuclear spin exchange process is developed. Preliminary data is presented and results are interpreted which display a significant contribution to the spin exchange interaction from the formation of the alkali-atom-noble-gas-atom diatomic molecules.

In Section III, the relaxation of polarized noble gas nuclei through the interaction of the nuclear quadrupole moment with electric field gradients is considered. A model for this interaction is presented which qualitatively explains various phenomena associated with the spin relaxation of Kr^{83}.

The work described in both Section II and III is part of a continuing effort. A more quantitative understanding of the associated phenomena is the aim of future work in these areas.

1.3 PROFESSIONAL PERSONNEL ASSOCIATED WITH THE PROGRAM

The principal investigator of these research efforts has been Dr. Charles H. Volk. This work has also been strongly supported by Dr. John G. Mark, Mr. Bruce C. Grover and Dr. Tae M. Kwon. We also wish to acknowledge the contributions of Mr. Howard E. Williams for the design, and Mr. Roger L. Meyer for the construction of various components of the apparatus used in this research effort.

SECTION II

EFFECTS OF ALKALI-ATOM-NOBLE-GAS-ATOM MOLECULES ON THE SPIN EXCHANGE PROCESS

2.1 INTRODUCTION

The spin exchange process between an alkali valence electron and a noble gas nucleus has been explained in terms of the contact-hyperfine interaction between an alkali atom and a noble gas nucleus. The effective hamiltonian governing this interaction has been shown to be:[1]

$$H_1 = \gamma \vec{I} \cdot \vec{S} \qquad (1)$$

where γ is the strength of the spin exchange interaction, $\vec{I}$ is the spin angular momentum of the noble gas nucleus and $\vec{S}$ is the spin angular momentum of the alkali valence electron. The equations of motion for observables of interest have been derived under H_1 for alkali and noble gas atoms interacting in binary type collisions,[2,3] and the experimental measurements were found to be in very good qualitative agreement.[3,4]

Recent measurements, however, of the alkali atom, noble gas nucleus, spin exchange cross section as a function of buffer gas pressure have demonstrated very strong effects which cannot be explained by a theory which contains binary collision effects only. These measurements indicate a significant role for the alkali-atom-noble-gas-atom Van der Waals molecule in the spin exchange process.

We will develop in this report the formalism to analyze the role of the Van der Waals molecules in our spin exchange measurements. We will adopt some simplifying assumptions, as was done in a previous report[3], in order to investigate the basics of the molecular interaction. Calculations are made for a system consisting of an atom with a single electron in a $^2S_{1/2}$ state and no nuclear spin (the alkali atom) and an atom with no electronic spin, $\vec{S} = 0$, and nuclear spin $\vec{I} = 1/2$ (the noble gas atom).

2.2 THE ALKALI-ATOM-NOBLE-GAS-ATOM DIATOMIC MOLECULE

The alkali-atom-noble-gas-atom Van der Waals molecule has been described by several authors[5-8] and recently its contributions to the relaxation of spin polarized alkali atoms have been discussed.[9,10] For the purposes of this report, we shall review the salient features of this diatomic system.

The alkali-atom-noble-gas-atom two-body problem reduces to a consideration of one body, with reduced mass:

$$\mu = M_A M_N/(M_A + M_N) \qquad (2)$$

where M_A is the mass of the alkali atom and M_N is the mass of the noble gas atom. The pair has energy, $E = h^2k^2/2\mu$, where k is the momentum of the reduced particle in the effective potential:

$$U_N(r,\Omega) = U(r,\Omega) + N(N + 1)h^2/2\mu\ r^2 \qquad (3)$$

where $U(r,\Omega)$ is the interatomic potential, r is the internuclear separation, N is the relative orbital angular momentum quantum number of the pair, and Ω is the solid angle. Low energy scattering experiments[11,12] have shown, for alkali atom, noble gas atom pairs investigated, that the interatomic potential is a central potential function; moreover, the Lennard-Jones[6-12] potential with two adjustable parameters, well depth and equilibrium separation, fits the experimental scattering data very well. The potential function is of the form:

$$U(r) = \epsilon_o\left[(r_m/r)^{12} - 2(r_m/r)^6\right] \qquad (4)$$

where r_m is the value of r at which U(r) is equal to its minimum value, ϵ_o.

A typical plot of energy versus internuclear separation is shown in Figure 2-1, for the effective potential $U_N(r)$. With reference to Figure 2-1, it is seen that the potential $U_N(r)$ can be divided into distinct areas labeled I, II, and III. Area I is defined such that $U_N \leq 0$. The systems in this region correspond to bound molecules, which are formed only in three body collisions and are destroyed in subsequent collisions of the complex with any other atom. Region II corresponds to quasibound molecules. Molecules in this region have energy levels such that $0 \leq E \leq E(N)$, and they are trapped by the centrifugal barrier. Since the energy levels are positive, quasibound molecules can be formed

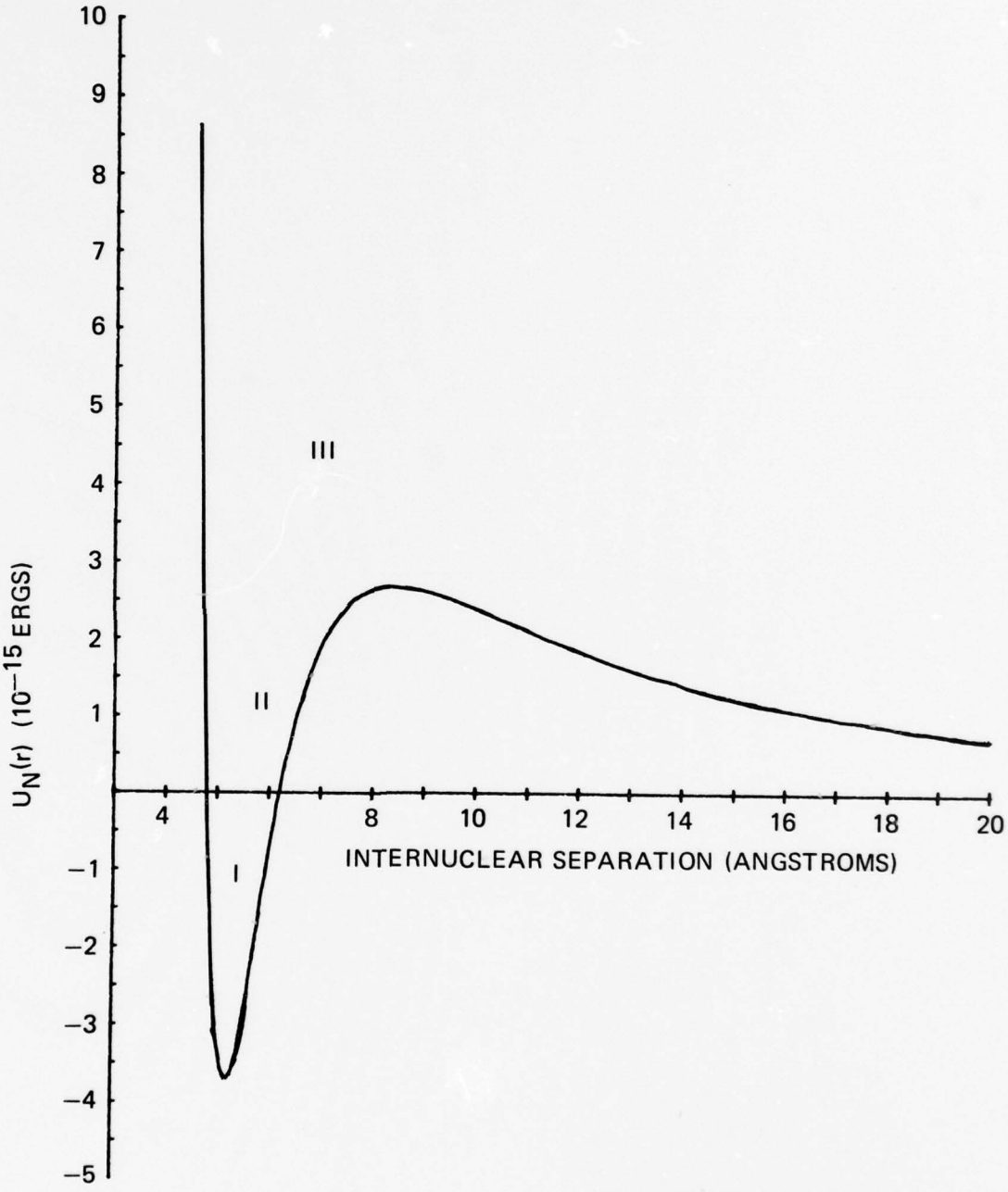

Figure 2-1. Alkali Noble Gas Interatomic Potential

in both two and three body collisions. In addition to the collisional destruction mode, quasibound molecules are characterized by a finite lifetime via quantum mechanical tunneling through the centrifugal barrier. If the half-life for decay through the barrier is greater than the average time between collisions then the quasibound molecules behave like bound states. When the time between collisions is long compared to the half-life for tunneling, then one must consider the phenomena of long-lived binary collisions whose properties differ from those of the sudden binary collisions. Finally, states in Region III are those of unbound alkali atom, noble gas atom pairs.

Theoretical determinations of potential parameters, such as the well depth and the equilibrium separation, are of two types: dispersion force calculations and pseudopotential calculations. The dispersion potential yields only information on the attractive nature of the internuclear potential and is of the form:

$$U(r) = - C_6/r^6 - C_8/r^8 \qquad (5)$$

C_6 and C_8 have been calculated for several alkali atom, noble gas atom pairs.[13] The dispersion force calculation is of limited value since no estimate on the minimum value of r for which the potential remains valid can be made.

Pseudopotential calculations have been done by Pascale and Vanderplanque[14] and Baylis.[15] The Baylis potential is such that it agrees with the dispersion force calculations at long range and with experimental determinations, in those cases for which these exist, near the bottom of the well. Table 2-1 lists some relevant molecular parameters based on the Baylis potential.

2.3 EFFECTS OF THE MOLECULAR LIFETIME ON THE EVOLUTION OF THE SYSTEM

We consider a system of alkali and noble gas atoms together with one or more buffer gases, typically N_2 and/or He, in the presence of some external magnetic field, which is used to define a quantization axis for this system.[16] The interaction between the alkali and noble gas atoms is assumed to be stochastic and governed by the hamiltonian defined in Eq. (1). Consider then the evolution of the wavefunction of the alkali atom, noble gas atom system from time t to time $t + \Delta t$. We divide the diatomic pairs into two classes:[9,17] (a) a fraction, $\Delta t/T_f$ that interact at an instant, t_o, where t_o is such that $t < t_o < t + \Delta t$ and T_f^{-1} is the rate of formation of the alkali-atom-noble-gas-atom interacting pairs, and (b) a fraction $(1 - \Delta t/T_f)$ which do not evolve during the same time interval. We impose the following restrictions $\Delta t \ll T_f$ and $\Delta t \gg T$, where T is the mean duration time of the interaction. The first relationship demands that the alkali atom, noble gas atom pair formation occurs in a time short compared to the time over which we look for variations in the

TABLE 2-1. SOME RELEVANT MOLECULAR PARAMETERS BASED ON THE BAYLIS POTENTIAL[a]

	Rb-Kr	Rb-Xe
$\epsilon_o \times 10^{18}$ ergs	1.46	2.02
$r_m \times 10^8$ cm	5.08	5.25
n_{o_B}	59,604	142,832
N_{max_B}	68	92
n_{o_T}	92,346	221,768
N_{max_T}	86	115
$(n_{AN}/n_A)_B \times 10^{+6}$ Torr	3.38	6.05
$(n_{AN}/n_A)_T \times 10^{+6}$ Torr @ 305°K	5.26	9.4

[a]The parameters we have listed in Table 2-1 are described below:

ϵ_o and r_m are the well depth and equilibrium separation for the alkali-noble-gas potential.[15]

n_{o_B} is the number of rotational states of the bound molecule.

N_{max_B} is the maximum angular momentum for the bound molecule; n_{o_T} and N_{max_T} are similarly defined for the total states of the molecule, bound plus quasibound.

(n_{AN}/n_A) is the concentration of molecules per alkali concentration per Torr of noble gas. The subscripts again denote the bound and total molecule. (The numbers in this table were calculated with the aid of References 7 and 8.)

wavefunction, while the second relation assumes that the wavefunction changes smoothly in time, since our observation is made over a time long compared to the duration of any interaction.

The time sequence may be pictured in the following way:

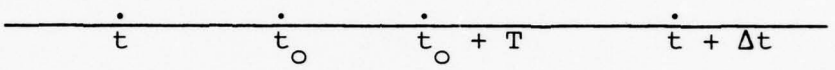

In the time intervals, $t_o - t$ and $t + \Delta t - t_o - T$, the system is governed by the 'free' hamiltonian, H_o, namely:

$$H_o = w_s S_z + w_I I_z \tag{6}$$

where w_s and w_I are the respective Larmor frequencies and h has been set to unity. In the interval T the systems evolve under the full hamiltonian:

$$H = H_o + H_1 \tag{7}$$

where H_1 is as defined in Eq. (1).

The wavefunction at time $t + \Delta t$ is then given in terms of the wavefunction at time t:

$$\Psi(t+\Delta t) = e^{-iH_o(t+\Delta t-t_o-T)} e^{-iHT} e^{-iH_o(t_o-t)} \Psi(t) \tag{8}$$

It is convenient at this point to transform the wavefunctions to the 'interaction picture', where:

$$\tilde{\Psi}(t+\Delta t) = e^{iH_o(t+\Delta t)} \Psi(t+\Delta t) \tag{9}$$

and

$$e^{iH_o t} \Psi(t) = \tilde{\Psi}(t) \tag{10}$$

Then by multiplying Eq. (8) through on both sides by $e^{iH_o(t+\Delta t)}$ and using Eq. (10), we find:

$$\tilde{\Psi}(t+\Delta t) = e^{iH_o t_o} e^{iH_o T} e^{-iHT} e^{-iH_o t_o} \tilde{\Psi}(t) \tag{11}$$

Eq. (11) then defines the evolution operator in the 'interaction picture':

$$\tilde{U}(t_o,T,H_1) = e^{iH_o t_o} e^{iH_o T} e^{-iHT} e^{-iH_o t_o} \tag{12}$$

If we designate the density matrix for the alkali atom, noble gas nucleus system as R, then in the 'interaction picture' the density matrix at time t+Δt is related to the density matrix at time t by:[2,3,9]

$$\tilde{R}(t+\Delta t) = (1-\Delta t/T_f)\, \tilde{R}(t) + \Delta t/T_f \langle \tilde{U}(t_o,T,H_1)\, \tilde{R}(t)\, \tilde{U}^t(t_o,T,H_1) \rangle_{ave} \tag{13}$$

where the first term on the right-hand side of Eq. (13) represents the probability that the system remains unchanged during the time interval Δt. The subscript 'ave' in the brackets indicates an average is to be performed over the stochastic variables t_o, T and H_1. We assume that all values of t_o in the interval Δt are equiprobable and we thus choose a particular value, that is we are able to rotate the evolution operator to form $V(T,H_1)$:

$$V(T,H_1) = e^{iH_o T} e^{-iHT} \tag{14}$$

Making the approximation:

$$\frac{d\tilde{R}(t)}{dt} \sim \frac{\tilde{R}(t+\Delta t) - \tilde{R}(T)}{\Delta t} \tag{15}$$

We can now write the differential equation for the density matrix of the alkali atom, noble gas nucleus system in the interaction:

$$\frac{d\tilde{R}(t)}{dt} = -(1/T_f)\left[\tilde{R}(t) - \langle V(T,H_1)\ \tilde{R}(t)\ V^t(T,H_1)\rangle_{ave}\right] \tag{16}$$

2.3.1 The Spin Exchange Equations

The density matrix of the system is, as previously defined,[2,3] the product of the density matrices, $\rho_A \otimes \rho_{NG}$, of the two subsystems, i.e., those of the alkali atom and the noble gas nucleus, respectively. We will designate the basis states $|m_I, m_S\rangle$ numerically as:

$$\left|\tfrac{1}{2}, \tfrac{1}{2}\right\rangle \qquad \left|\tfrac{1}{2}, -\tfrac{1}{2}\right\rangle \qquad \left|-\tfrac{1}{2}, \tfrac{1}{2}\right\rangle \qquad \left|-\tfrac{1}{2}, -\tfrac{1}{2}\right\rangle$$

1 2 3 4

and thus the elements of the density matrix, R, can be expressed without cumbersome notation.

We have assumed that the density matrix of the system can be represented in terms of the products of the basis states of the subsystems, since the coupling between the alkali and noble gas atoms in the Van der Waals molecule is weak (see Table 2-1). This is not a bad approximation as long as the wavefunction overlap effects are taken into account.[1]

We define the following:

$$A = e^{-i\gamma\, T/4} \tag{17a}$$

$$B = e^{iDT}\left(\cos^2 X\, e^{-iw^+T} + \sin^2 X\, e^{-iw^-T}\right) \tag{17b}$$

$$C = e^{iDT}(\cos X)(\sin X)\left(e^{-iw^+T} - e^{-iw^-T}\right) \tag{17c}$$

$$E = e^{-iDT}(\cos X)(\sin X)\left(e^{-iw^+T} - e^{-iw^-T}\right) \tag{17d}$$

and

$$F = e^{-iDT}\left(\cos^2 X\, e^{-iw^-T} + \sin^2 X\, e^{-iw^+T}\right) \tag{17e}$$

where

$$D = (w_I - w_s)/2 \tag{18a}$$

$$w^{\pm} = \gamma/4 \pm \sqrt{\gamma^2/4 + D^2/4} \tag{18b}$$

$$\tan X = D + \sqrt{\gamma^2/4 + D^2/4} \Big/ (\gamma/2) \tag{18c}$$

The time evolution part of the density matrix, $V\tilde{R}V^t$ can then be written as shown in Figure 2-2.

The observables of interest for the noble gas nucleus are $\langle I_z \rangle$ and $\langle I^+ \rangle$, which are the expectation values of the longitudinal and transverse polarization of the noble gas nucleus, respectively. These are given in terms of the density matrix:

$$\langle I_z \rangle = Tr\left[I_z R\right] = \frac{1}{2}\left(\rho_{NG\ \frac{1}{2}\frac{1}{2}} - \rho_{NG\ -\frac{1}{2}-\frac{1}{2}}\right) \tag{19}$$

and

$$\langle I^+ \rangle = Tr\left[I^+ R\right] = \rho_{NG\ \frac{1}{2}-\frac{1}{2}} \tag{20}$$

where I_z and I^+ are the corresponding operators.

$$
\begin{bmatrix}
\tilde{A}\tilde{R}_{11}A^* & \tilde{A}\tilde{R}_{12}B^* + \tilde{A}\tilde{R}_{13}C^* & \tilde{A}\tilde{R}_{12}E^* + \tilde{A}\tilde{R}_{13}F^* & \tilde{A}\tilde{R}_{14}A^* \\
\tilde{B}\tilde{R}_{21}A^* + \tilde{C}\tilde{R}_{31}A^* & \tilde{B}\tilde{R}_{22}B^* + \tilde{B}\tilde{R}_{23}C^* + \tilde{C}\tilde{R}_{32}B^* + \tilde{C}\tilde{R}_{33}C^* & \tilde{B}\tilde{R}_{22}E^* + \tilde{B}\tilde{R}_{23}F^* + \tilde{C}\tilde{R}_{32}E^* + \tilde{C}\tilde{R}_{33}F^* & \tilde{B}\tilde{R}_{24}A^* + \tilde{C}\tilde{R}_{34}A^* \\
\tilde{E}\tilde{R}_{21}A^* + \tilde{F}\tilde{R}_{31}A^* & \tilde{E}\tilde{R}_{22}B^* + \tilde{E}\tilde{R}_{23}C^* + \tilde{F}\tilde{R}_{32}B^* + \tilde{F}\tilde{R}_{33}C^* & \tilde{E}\tilde{R}_{22}E^* + \tilde{E}\tilde{R}_{23}F^* + \tilde{F}\tilde{R}_{32}E^* + \tilde{F}\tilde{R}_{33}F^* & \tilde{E}\tilde{R}_{24}A^* + \tilde{F}\tilde{R}_{34}A^* \\
\tilde{A}\tilde{R}_{41}A^* & \tilde{A}\tilde{R}_{42}B^* + \tilde{A}\tilde{R}_{43}C^* & \tilde{A}\tilde{R}_{42}E^* + \tilde{A}\tilde{R}_{43}F^* & \tilde{A}\tilde{R}_{44}A^*
\end{bmatrix}
$$

Figure 2-2. Time Evolution Term of the Density Matrix, $\tilde{V}\tilde{R}\tilde{V}^t$

In the limit of low magnetic field, which is a reasonable limit for the noble gas nucleus since the Larmor frequencies are much lower than the spin exchange energy for the magnetic fields at which we work, we find the spin exchange equations from Eqs. (16), (19) and (20):

$$\langle \dot{I}_z \rangle = -(1/T_f)\left[\langle I_z \rangle - \langle S_z \rangle\right] \sin^2(\gamma T/2)_{ave} \tag{21}$$

and

$$\langle \dot{I}^+ \rangle = -(1/T_f)\left[\langle I^+ \rangle - \langle S^+ \rangle\right] \sin^2(\gamma T/2)_{ave}$$

$$-i\left[\langle S_z \rangle \langle I^+ \rangle - \langle I_z \rangle \langle S^+ \rangle\right] \sin(\gamma T)_{ave} \tag{22}$$

We average over the collision duration by assuming that the primary effect of the molecular formation on the spin exchange process is that of extending the life of the interaction only. Eqs. (21) and (22) become after averaging:

$$\langle \dot{I}_z \rangle = -(1/T_f)\,\frac{\gamma^2\tau^2}{1+\gamma^2\tau^2}\left[\langle I_z \rangle - \langle S_z \rangle\right] \tag{23}$$

$$\langle \dot{I}^+ \rangle = -(1/Tf)\,\frac{\gamma^2\tau^2}{1+\gamma^2\tau^2}\left[\langle I^+ \rangle - \langle S^+ \rangle\right]$$

$$+\,(i/T_f)\,\frac{\gamma\tau}{1+\gamma^2\tau^2}\left[\langle S_z \rangle \langle I^+ \rangle - \langle I_z \rangle \langle S^+ \rangle\right] \tag{24}$$

where τ represents the mean life of the interaction state. For the case of low external magnetic field, Eqs. (23) and (24) have exactly the same form as for the binary collision case.

2.3.2 The Exchange Rate

From Eqs. (23) and (24) we define the exchange rate for the exchange of spin angular momentum from the alkali atom to the noble gas nucleus:

$$T_{ex}^{-1} = T_f^{-1}\left[\frac{\gamma^2\tau^2}{2(1+\gamma^2\tau^2)}\right] \tag{25}$$

In addition a spin exchange cross section can be defined as:

$$T_{ex}^{-1} = N_A\ \sigma_{ex}\ V_{rel} \tag{26}$$

where N_A is the alkali number density, σ_{ex} is the exchange cross section and V_{rel} is the relative velocity between the alkali and noble gas atoms.

Eq. (25) is true, however; only if a single exchange process is present, e.g., binary collisions. In general one would expect three types of processes, so that the total exchange rate could be written as:

$$T_{ex}^{-1} = T_{ex_{bound}}^{-1} + T_{ex_{quasi\text{-}bound}}^{-1} + T_{ex_{binary}}^{-1} \tag{27}$$

where the first term in Eq. (27) represents the exchange rate through bound molecular complexes, the second term is the contribution of the quasi-bound molecules to the exchange process

and the third term is spin exchange due to binary, alkali atom, noble gas atom collisions.

We now consider each term as a function of the buffer gas pressure, with the form of the exchange rate for each process being given by Eq. (25):

a. Bound state molecules (alkali-atom-noble-gas-atom which exist in Region I of Figure 2-1): As was discussed in Section 2.2, the bound complexes are formed in three-body collisions only, as a result of conservation of energy and thus for a given alkali and noble gas atom concentration, the formation rate, T_f^{-1}, is proportional to the buffer gas density. Since the binding energy of these Van der Waals molecules is less than a kT, the molecular state exists only until its next collision with any atom, which, due to the concentration of constituents in our cells, makes it inversely proportional to the buffer gas density. The overall effect then, for sufficiently low noble gas densities, is that at low buffer gas densities the exchange rate is proportional to the buffer gas density, and for high buffer gas densities, is inversely proportional to the buffer gas density.

b. Quasi-bound molecules (complexes in Region II of Figure 2-1): The quasi-bound molecules are formed in two ways: (1) through two-body alkali noble gas atom resonant collisions in which tunneling through the centrifugal barrier takes place, and (2) in three-body collisions, in the same manner as for the formation of the bound state molecules. In case '1' the formation rate is constant in buffer gas density while in case '2' the formation rate is proportional to the buffer gas density. The destruction of the quasi-bound molecules can also occur in two ways: (1) decay of the resonant state via tunneling back through the barrier, and (2) in a collision of the quasi-bound complex with another atom as in the case of the bound molecules. The different creation and destruction modes for the quasi-bound molecules result in four different types of buffer gas density dependencies in the exchange rate. However, two of these dependencies are indistinguishable from the other two exchange processes, that is, a quasi-bound molecule formed in a three-body collision and then destroyed in a subsequent collision with another atom behaves like a bound molecule, and a quasi-bound molecule formed through tunneling which then decays through tunneling has the same density dependence as a binary collision. In addition, previous experimental

work has suggested that the quasi-bound molecules involving an alkali and one of the heavier noble gases (Ar, Kr, Xe) do not contribute significantly in alkali, noble gas interactions. We assume then that any buffer gas density dependence of the exchange rate due to the quasi-bound molecules will be very weak.

c. Alkali atom, noble gas atom, binary collisions. This process leads to an exchange rate that is independent of buffer gas density.

Considering then the exchange rate through only bound state molecules and binary collisions, we parameterize the exchange rate as a function of buffer gas density, in the limit of low noble gas densities, as:

$$T_{ex}^{-1} = \frac{abn_b}{n_b^2 + b} + c \qquad (28)$$

where a, b and c are constants and n_b is the density of the buffer gas. Examining Eq. (28) then, we would expect the exchange rate to increase linearly in n_b for low buffer gas densities and then decrease as $1/n_b$ to the constant binary rate in the limit of high buffer gas densities, if the alkali atom, noble gas nucleus, spin exchange rate is influenced by the presence of the Van der Waals molecules.

2.4 EXPERIMENTAL RESULTS

The experimental apparatus and data acquisition procedure have been described previously.[3] In brief, the Rb cell is mechanized as a magnetometer as described by Cohen-Tannoudji, et al,[18] and thus the precession of the noble gas nuclei is detected as an oscillating magnetic field.

Sample data taken in this manner is displayed in Figure 2-3. This particular data was from a cell containing natural Rb, 15 Torr N_2, 30 Torr He and 0.5 Torr Xe^{129}. The horizontal axis on all three plots represents time. The full length of each run was approximately 500 seconds. The vertical axis on each plot is the amplitude of the signal. Note that the middle plot has a scale larger than the other two by a factor of two. The top plot in Figure 2-3 represents data taken at 38°C, the middle plot that taken at 58°C and the bottom plot that taken at 74.5°C.

2.4.1 Data Reduction

We typically perform two types of experiments: one in which we examine the longitudinal (T_1) pumping of the noble gas nuclei and the other in which we observe the transverse (T_2) decay of the nuclear spin system. Longitudinal effects, which are represented by Eq. (23), are measured by pumping the nuclear spin system, through spin exchange, for various specified lengths of time and then recording the amplitude of the nuclear magnetization.

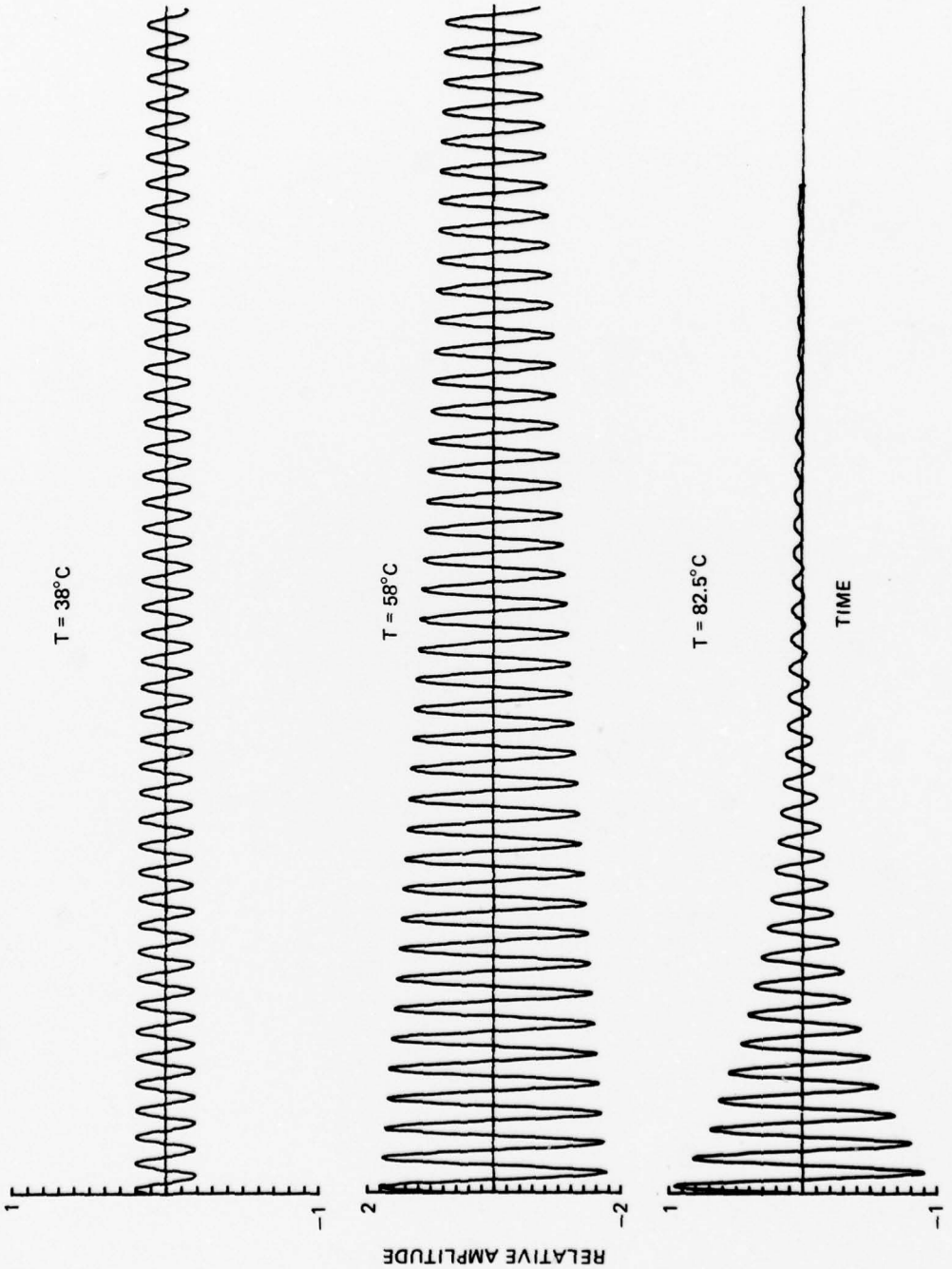

Figure 2-3. Xe^{129} Decay Signal at Three Temperatures

Assuming that the nuclear magnetization obeys a simple exponential pumping law:

$$M(t) = M_o(1 - e^{-t/T_p}) \tag{29}$$

one can fit the experimental data at a particular temperature for the 'pump rate', T_p^{-1}; represented in Figure 2-4. Repeating this as a function of cell temperature, and assuming the dominant temperature dependence of the pump rate is due to the spin exchange process, with the temperature dependence given by Eq. (26), we have:

$$T_p^{-1}(T) \approx T_1^{-1} + T_{1ex}^{-1}(T) \tag{30}$$

and thus by performing a linear fit to the pump rate data as a function of N_A/V_{rel}, one can find a value for T_1^{-1}, the longitudinal relaxation rate, and the spin exchange cross section for any temperature, as shown in Figure 2-5. We note here that we fit the pump rate data as a function of N_A/V_{rel} and not $N_A V_{rel}$, as might be expected from Eq. (26), since by Ref. 1 the cross section for spin exchange is proportional to V_{rel}^{-2}.

In our particular experiments, the alkali is Rb, and we use the saturated rubidium density formula for the number density:[19]

$$\log N_{Rb} = -4560/T - 2.45 \log(T) + 30.98 \tag{31}$$

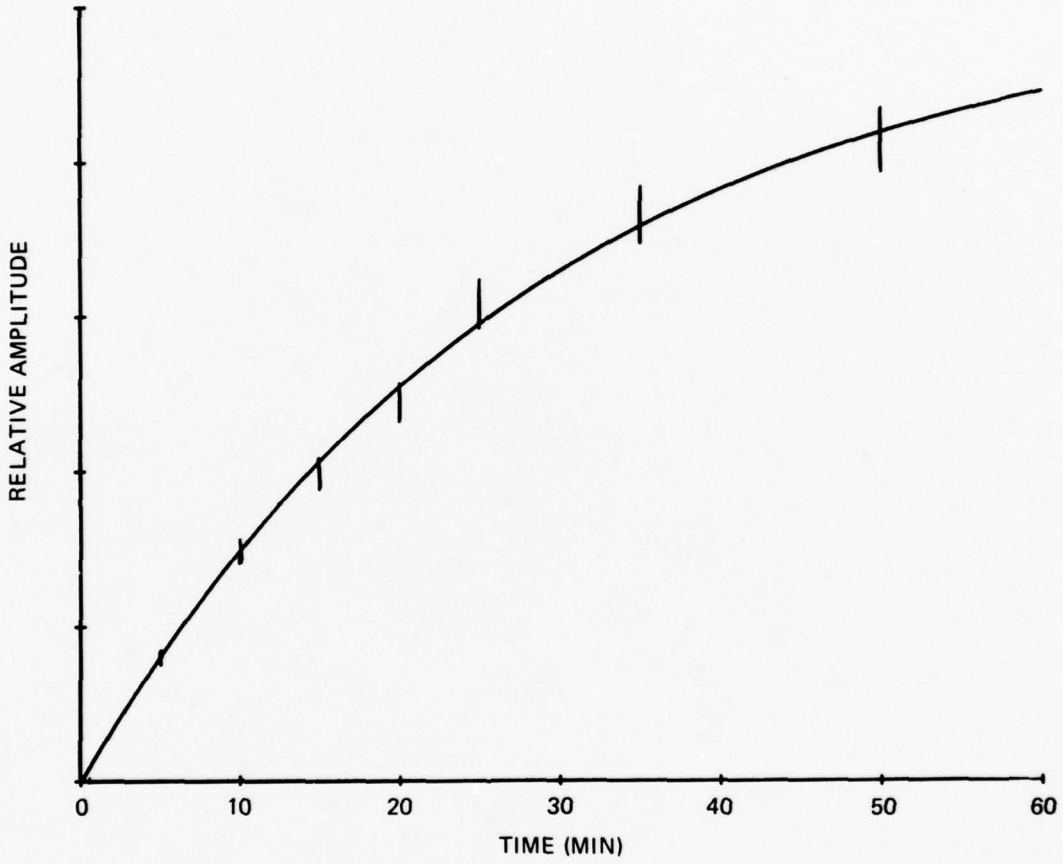

INITIAL AMPLITUDE DATA IS FIT TO THE FUNTIONAL FORM GIVEN IN EQ. (29). THIS PLOT REPRESENTS DATA TAKEN FROM A CELL CONTAINING NATURAL Rb, 15 TORR N_2, 100 Torr He AND 0.5 Torr Xe (129) AT A TEMPERATURE OF 49.2°C. A LEAST SQUARES FIT OF THE DATA YIELDED A PUMP TIME, T_p = 1727, THE ERROR BARS REPRESENT A 5 PERCENT UNCERTAINTY IN THE AMPLITUDE.

Figure 2-4. Initial Noble Gas Signal Amplitude Versus Pump Time

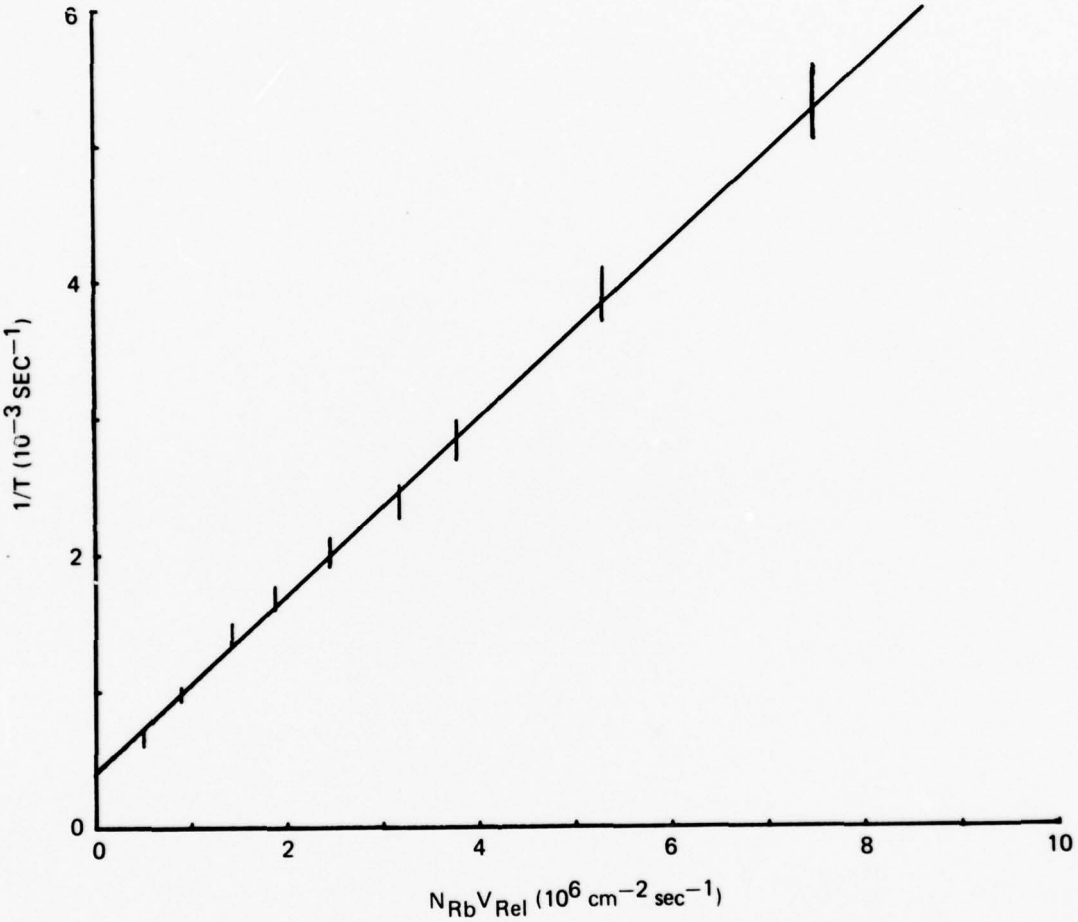

INTERCEPT REPRESENTS THE TEMPERATURE INDEPENDENT DECAY RATE AND THE SLOPE YIELDS INFORMATION ON THE SPIN EXCHANGE CROSS SECTION. ERROR BARS REPRESENT A 5 PERCENT UNCERTAINTY IN THE DECAY RATE. DATA IS TAKEN FROM A CELL CONTAINING Rb(87), 20.5 Torr N_2 AND 0.05 Torr Xe(129). LEAST SQUARES FIT YIELDED A TEMPERATURE INDEPENDENT RATE OF 4.5×10^{-4} sec^{-1} AND $\sigma_{ex}V^2_{rel} = 6.1 \times 10^{-10}$ cm^4 sec^{-2}.

Figure 2-5. Noble Gas Decay Rate Versus Rb Density Times Relative Velocity

where T is the cell temperature in degrees Kelvin. The transverse decay rate of the nuclear spin system is found by fitting the data such as that displayed in Figure 2-3 to a decaying exponential function. Referring to Eq. (24), one finds that if the T_2 of the alkali spin system is much shorter than that of the nuclear spin system, then the decay of the nuclear levels and the alkali electronic levels effectively decouple and Eq. (24) becomes:

$$\langle \dot{I}^+ \rangle = -(1/T_{ex}) \langle I^+ \rangle + (i/T_{ex}) \langle S_z \rangle \langle I^+ \rangle \qquad (32)$$

The real part of Eq. (32) represents the transverse decay of the nuclear levels. Assuming that other contributions to the transverse rate can be represented by a single decay rate, we find that the nuclear spin decay to be given by:

$$\langle \dot{I}_x \rangle = - \left[T_{ex}^{-1} + (T_2')^{-1} \right] \langle I_x \rangle \qquad (33)$$

where $T_2^{-1} = T_{ex}^{-1} + (T_2')^{-1}$ is the total transverse decay rate and $(T_2')^{-1}$ is the temperature independent component of the total transverse rate. We again assume, as was done for the longitudinal pumping, that the dominant temperature dependence in the decay rate is due to the exchange term. Performing a linear fit of T_2^{-1} as a function of N_A/V_{rel} yields the temperature independent T_2 rate, T_2', and the transverse exchange cross section.

By Eqs. (23) and (24) the exchange cross section, found by analyzing the longitudinal pumping, is equal to that found by the transverse decay rate.

2.4.2 Analysis of the Molecular Effects

We have initiated spin relaxation measurements of Xe^{129} in a series of cells designed to yield information concerning the role of the Rb-Xe diatomic molecules in the spin exchange process. The series of cells contain Rb^{87} metal, 0.05 Torr Xe^{129} and N_2 from 4.3 Torr to 80 Torr. Results of the measurements are displayed in Figure 2-6 where we have plotted $\sigma_{ex} v_{rel}^2$ versus N_2 pressure. The bars on the data points represent a 15 percent uncertainty both in N_2 pressure and $\sigma_{ex} v_{rel}^2$, and are intended only as a gauge of the validity of the Least Squares fit, solid line, of the data points to Eq. (28). Although the agreement between our model and experimental results in this preliminary measurement is not as good as would be needed in order to reach definitive conclusions, we are at this time able to make some basic observations:

a. The spin exchange process between the alkali valence electron and the noble gas nucleus is a function of the buffer gas density in the cell. This fact is consistent with the model in which the Van der Waals molecules have a significant contribution to the exchange process.

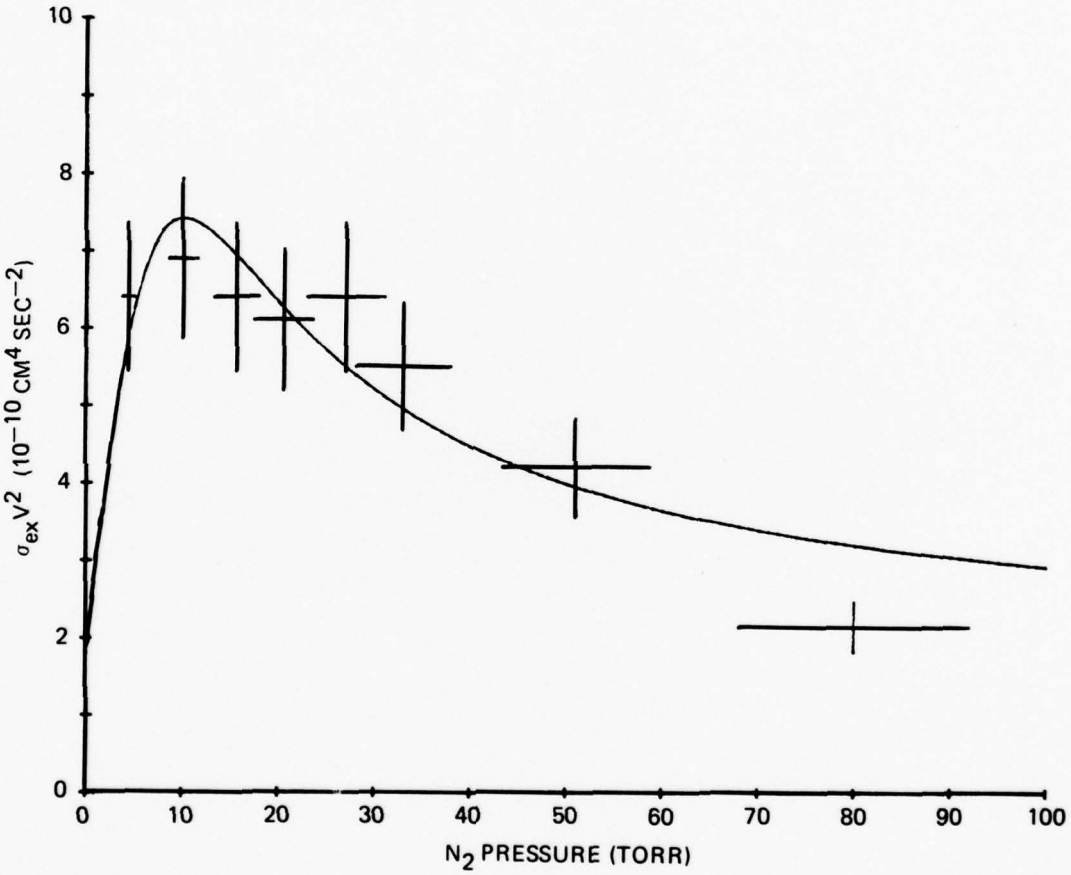

ERROR BARS REPRESENT A 15 PERCENT UNCERTAINTY IN BOTH THE BUFFER GAS PRESSURE AND THE EXCHANGE CROSS SECTION INFORMATION.

Figure 2-6. Rb^{87} - Xe^{129} Spin Exchange Cross Section as a Function of N_2 Pressure

b. We obtained three parameters related to the three-body collision rate, the interaction strength times the molecular lifetime, and the binary spin exchange cross section from a Least Squares fit of our data to Eq. (28):

(1) We obtained the three-body collision rate of Rb, Xe and N_2 per Xe atom. Evaluating this rate at 60°C and 1 Torr N_2 we find:

$$T_f^{-1} = 4.5 \times 10^{-4} \text{ sec}^{-1} \tag{34}$$

Major[2] argued, based on a hard sphere collision model, that an upper bound for the termolecular collision rate per Xe atom at 60°C per Torr of N_2 is:

$$T_f^{-1} = 2.5 \times 10^{-3} \text{ sec}^{-1} \tag{35}$$

Our estimate of the molecular formation rate seems to be in reasonable agreement with that deduced by Major.

(2) The average strength of the interaction multiplied by the duration of the interaction per Torr N_2 we found to be:

$$\langle \gamma \rangle \tau \sim 10 \tag{36}$$

If we assume that the lifetime of the molecular state is limited by N_2 collisions, we can use the same gas kinetic arguments as those employed in (1) to estimate τ:

$$\tau = 0.5 \times 10^{-7} \text{ sec/Torr } N_2 \tag{37}$$

Substituting this value into Eq. (36) we obtain an estimate for the average strength of the interaction during the molecular lifetime:

$$\langle\gamma\rangle \sim 2 \times 10^{8} \text{ sec}^{-1} \tag{38}$$

The strength is in reasonable agreement with what had been previously estimated for the binary collisions.[2,3]

(3) The data fit yields a spin exchange cross section for the Rb-Xe^{129} binary collisions:

$$\sigma_{ex_B} \cong 1.5 \times 10^{-19} \text{ cm}^2 \tag{39}$$

This value is in excellent agreement with cross sections measured for Rb-Xe^{129} in cells buffered with 500 Torr He, where one would expect binary collision contributions only.[4]

We have attributed the scatter in our experimental data to two main sources of difficulty:

a. It was discovered in the process of filling this present series of cells that our buffer gas filling procedure could result in very large uncertainties in the fill pressure of the buffer gas. A new procedure has been devised and a second series of cells is being completed for which these present measurements will be repeated.

b. The non-spin-exchange part of the T_2 relaxation rate for Xe^{129} is mainly due to the interaction of the dipole moment of the Xe nucleus with the magnetic field gradients present in the cell. This relaxation is of the form:[20]

$$T_{2_G}^{-1} = \gamma^2 D\, G^2 \tau_v^2 \tag{40}$$

where D is the diffusion coefficient of the Xe through the buffer gas, G is the magnetic field gradient along the quantization axis and τ_v is the diffusion time from wall to wall of the atom in the cell. We approximate τ_v by:[21]

$$\tau_v = R^2/\pi D \tag{41}$$

where R is the radius of the cell and we take the pressure and temperature of the diffusion coefficient as[22]

$$D = \frac{D_o P_o}{p} (T/T_o)^{\alpha} \tag{42}$$

where p is the pressure of the buffer gas, p_o is standard pressure, T is the temperature of the cell, T_o is 273°K and α is a parameter between 1.75 and 2. The spin relaxation due to magnetic field gradients can then be written as:

$$T_G^{-1} = K\ P/T^{\alpha} \tag{43}$$

where K is some constant. From Eq. (43) one can see that in very highly buffered cells, relaxation due to magnetic field gradients can dominate the spin exchange process and thus cause large errors in the spin exchange measurements.

To determine whether magnetic field gradient relaxation was a significant part of the total observed relaxation in our cells, we plotted the T_2 rate intercept found in extracting the spin exchange information (see Figure 2-5) versus the N_2 pressure, as shown in Figure 2-7. The solid line in Figure 2-7 represents a Least Squares fit of the data points as a function of N_2 pressure according to Eq. (43). From the slope of the line, we have inferred that there is a magnetic field gradient in our apparatus of approximately 4 μG/cm. This implies that our present data

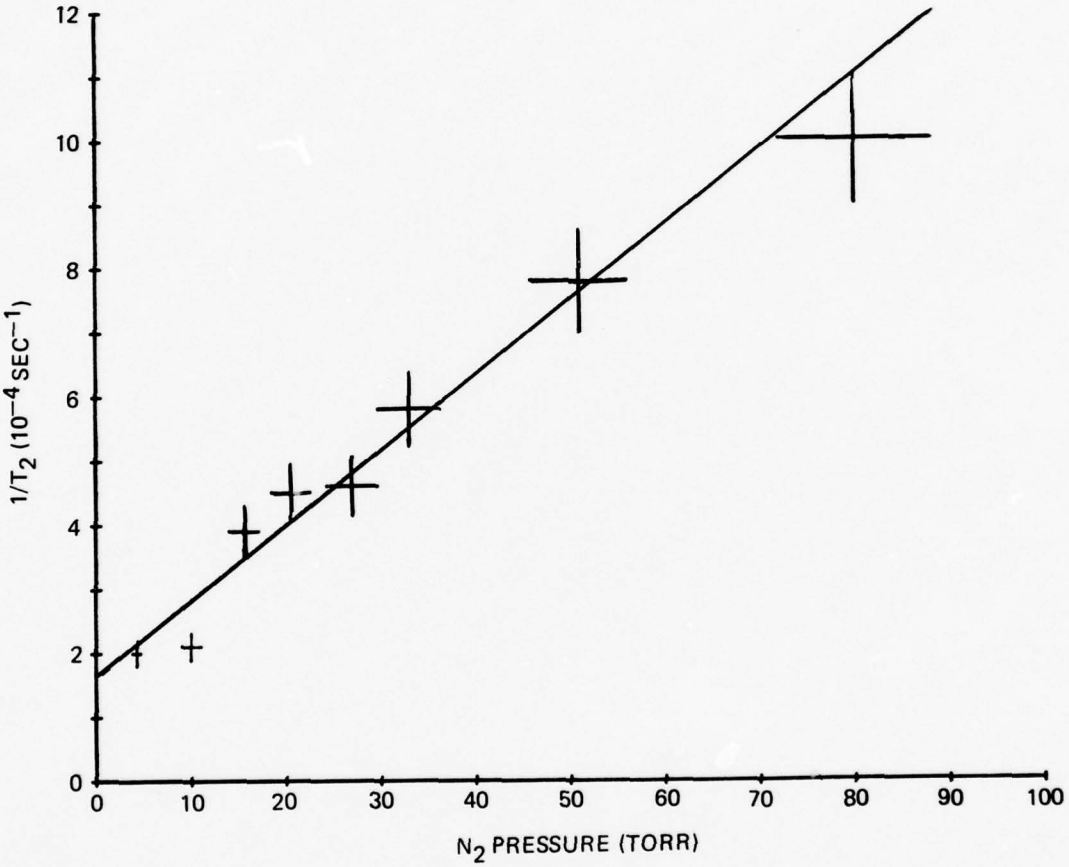

ERROR BARS REPRESENT A 15 PERCENT UNCERTAINTY IN BOTH THE N_2 PRESSURE AND THE DECAY RATE.

Figure 2-7. Decay Rate Intercept Versus N_2 Buffer Pressure

reduction technique probably loses validity around N_2 pressures of 100 Torr due to the significant temperature contributions as shown in Eq. (43). At the present time we are working to reduce this magnetic field gradient in our apparatus by means of gradient compensating coils.

2.5 SUMMARY

We have developed a model for the role of the Rb-Xe Van der Waals molecular complexes in the Rb electronic Xe nuclear spin exchange interaction. The preliminary measurements of the spin exchange parameters have revealed a significant contribution to the spin exchange process from the formation of the Van der Waals molecules however, we are not able to make a definitive comparison between the model and the experimental results at this time.

2.6 CONSIDERATIONS FOR FUTURE WORK

Our aim is to reduce those sources of error in our apparatus and measurement technique which have been identified as a result of this series of measurements. Similar measurements will be made extending the buffer gas regime out to several hundred Torr in order to check the limiting regions of our model.

Future work will also involve developing an understanding of the role of both the alkali nuclear spin and the noble gas spin by considering similar measurements employing both Rb^{85} and Xe^{131}.

2.7 BIBLIOGRAPHY FOR SECTION II

1. R.M. Herman, Phys. Rev. 4A, 137 (1965).
2. F.G. Major, Litton Subcontract Report, Subcontract No. WC376807 (unpublished).
3. C.H. Volk, B.C. Grover and E. Kanegsberg, AFOSR, Annual Technical Report (1978)(unpublished).
4. B.C. Grover, Phys. Rev. Lett. 40, 391 (1978).
5. J.O. Hirschfelder, C.F. Curtiss and R.B. Bird, Molecular Theory of Gases and Liquids, John Wiley and Sons, Inc., New York, 1954.
6. D.E. Stogryn and J.O. Hirschfelder, J. Chem. Phys. 31, 153 (1959).
7. G.D. Mahan and M. Lapp, Phys. Rev. 179, 19 (1969).
8. G.D. Mahan, J. Chem. Phys. 52, 258 (1970).
9. C.C. Bouchiat, M.A. Bouchiat and L.C.L. Pottier, Phys. Rev. 181, 144 (1969); C.C. Bouchiat and M.A. Bouchiat, Phys. Rev. 2A (1976).
10. F.A. Franz and C. Volk, Phys. Rev. 14A, 1711 (1976); Phys. Rev. 18A, 599 (1978).
11. R.B. Bernstein and J.T. Muckerman, Theoretical Chemistry Institute, University of Wisconsin, Report No. 200, 1967.
12. F. von Busch, J.J. Strunk and C. Schlier, Z. Phys. 199, 518 (1967).
13. A. Dalgarno and W.D. Davison, Mol. Phys. 13, 479 (1967).

14. J. Pascale and J. Vanderplanque, J. Chem. Phys. 60, 479 (1967).

15. W.E. Baylis, J. Chem. Phys. 51, 2265 (1969); corrected values by private communication.

16. The results of the section are very similar to those presented in a previous report[3], however, the underlying assumptions are significantly different and this new derivation was done in order to assure validity of the relationships involved in the description of the spin exchange process.

17. Francis Hartmann and Francoise Hartmann-Boutron, Phys. Rev. 2A, 1885 (1970).

18. C. Cohen-Tannoudji, J. Dupont-Roc, S. Haroche and F. LaLoe, Rev. de Phys. Appl. 5, 95 (1970); 5, 102 (1970).

19. C.J. Smithells, Metals Reference Book, Vol. 2 (Butterworths, London, 1962), p. 655.

20. S.P. Dovgopol, V.P. Putyrskii and S.L. Votyakov, Opt. Spectr. 35, 586 (1973).

21. W. Franzen, Phys. Rev. 115, 850 (1959).

22. American Institute of Physics Handbook, Second Edition (McGraw-Hill, New York, 1963), p. 2-237.

SECTION III

NOBLE GAS RELAXATION EFFECTS

3.1 INTRODUCTION

Recent measurements in our laboratory of the transverse decay rate of Kr^{83} showed that the decay of the nuclear polarization is dependent on the particular orientation of the NMR cell in the experimental apparatus. This effect was previously observed[1,2] in the relaxation of Hg^{201}. The particular orientation of the Hg^{201} cell which resulted in the longest T_2 decay time of the Hg polarization was termed the "magic angle" where the angle was between the cell axis and the externally applied magnetic field.[1] No such angular effects have been observed in either Xe^{129} or Hg^{199} both of which have nuclear spin I = 1/2, this suggests that the angular effect results from quadrupolar type interactions present in Kr^{83} and Hg^{201} decay. In this section we will consider possible relaxation phenomena associated with quadrupolar interactions present in nuclei with spin greater than 1/2, developing particular expressions for nuclear spin species I = 9/2, Kr^{83}, and I = 3/2, Xe^{131} and Hg^{201}.

3.2 THE EXPERIMENTAL OBSERVATIONS

Typical precessional decay data for a Kr^{83} sample is displayed in Figures 3-1 and 3-2. This particular sample contained natural Rb metal, 150 Torr N_2 and 5 Torr Kr^{83} in a 1 ml Corning 1720 glass cell. Figures 3-1 and 3-2 represent data taken at

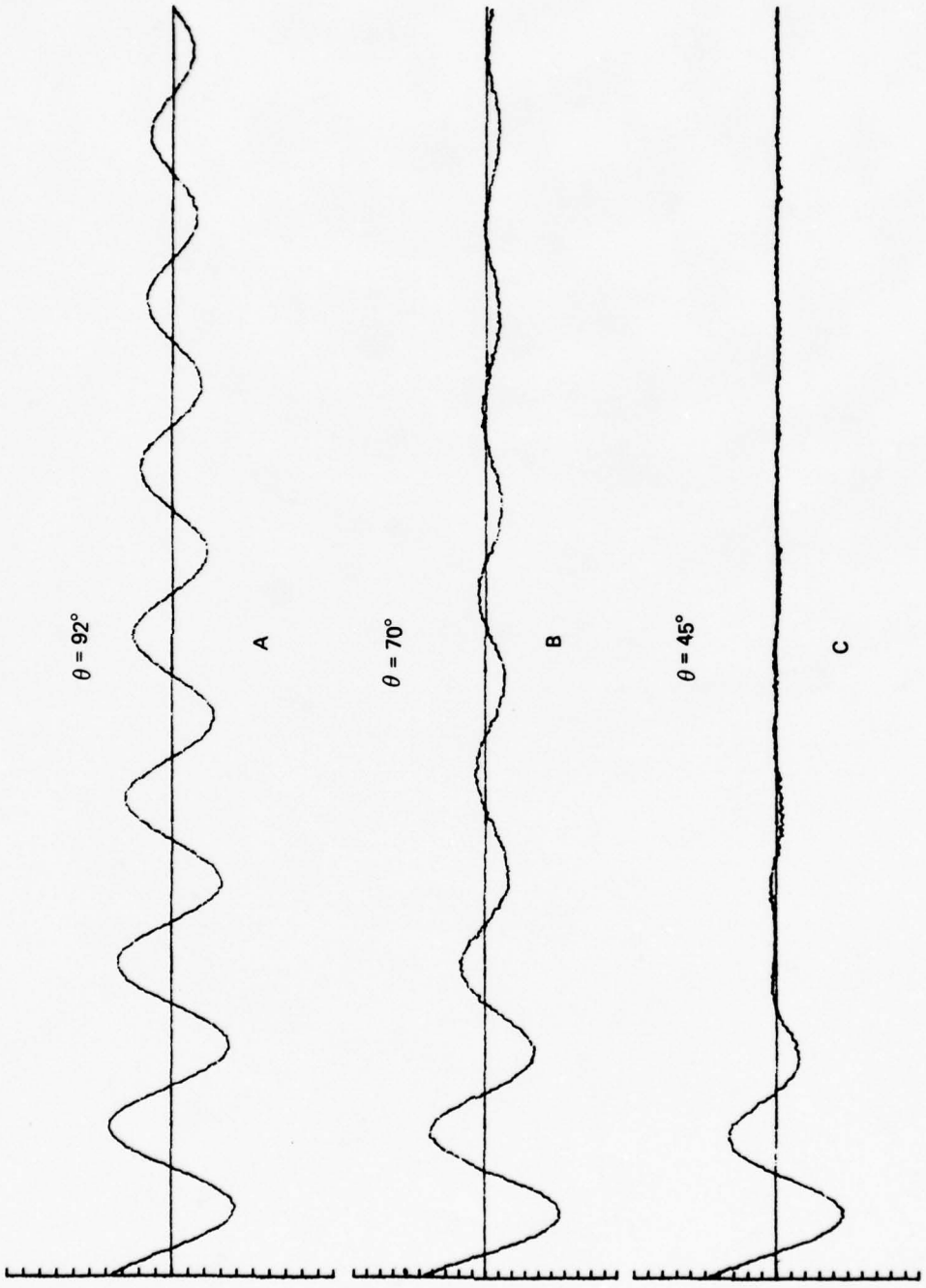

Figure 3-1. Kr Decay Signal Showing Relative Amplitude Versus Time for a 500 Second Data Run
θ Indicates the Relative Orientation of the Cell in the Apparatus

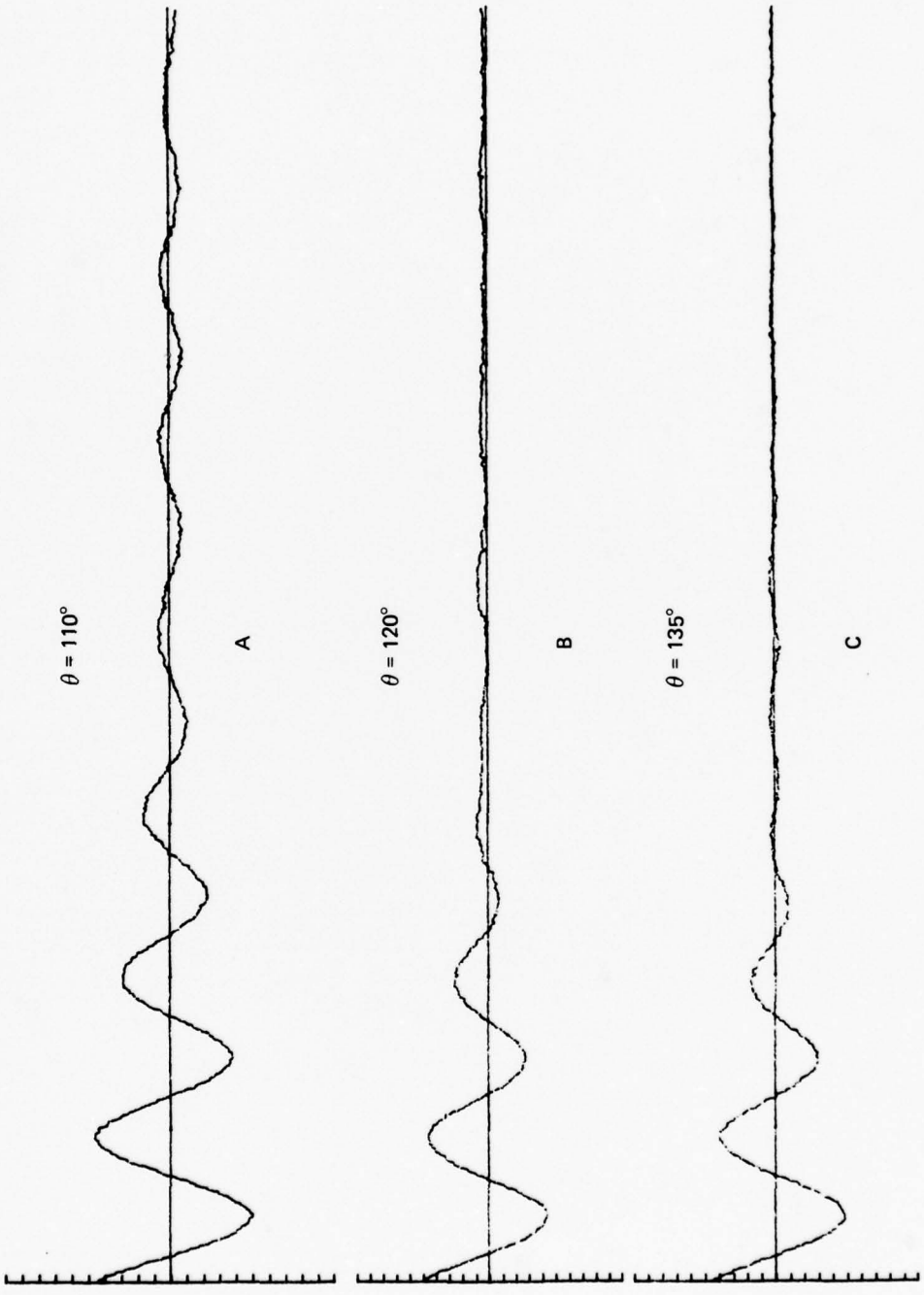

Figure 3-2. Kr Decay Signal Showing Relative Amplitude Versus Time for a 500 Second Data Run
θ Indicates the Relative Orientation of the Cell in the Apparatus

the same temperature, approximately 60°C, after an initial constant pump time with each plot corresponding to a different orientation of the cell in the experimental apparatus. The data stream in each plot is 500 seconds long. The angle indicated on each plot is taken between the cell axis and the externally applied magnetic field. The cell axis was taken to be along a line that passes symmetrically through the tip-off region of the cell as a matter of convenience.

3.2.1 General Features of the Data

We enumerate general observations concerning the data:

a. T_2 decay of the Kr^{83} spin system is a function of angular orientation of the cell in the experimental apparatus.

b. The Kr signals cannot be solely described by an exponential decay. In addition, the non-exponential character of the decay is a function of angle.

c. The precession frequency is a function of time and cell orientation. This can be seen by comparing Figures 3-1a and 3-1b. Also comparing Figures 3-1a and 3-1c one sees an indication of a possible phase reversal in the second cycle of Figure 3-1c.

d. The decay characteristics at a particular angle designation are a function of the position of the Rb metal reservoir in the cell. In the sample shown, the magic

angle for the cell was at or near 92 degrees. The magic angle for the cell can therefore be changed by moving the Rb distribution on the cell walls.

e. Previous measurements of the Kr decay characteristics as a function of cell size demonstrated a significant contribution to the relaxation processes from wall effects.

f. The initial amplitudes appear to be constant as a function of angle, implying that the angular effect does not significantly contribute to the T_1 processes of the Kr spin system.

3.3 TRANSVERSE RELAXATION EFFECTS

Transverse (i.e., T_2) relaxation refers to the loss of phase coherence in a precessing spin system. Spin de-phasing in a quadrupolar interaction can arise through both an inhomogeneous broadening of the nuclear Zeeman levels and transitions among the energy levels.[3]

3.3.1 Level Shifts Due to a Quadrupolar Interaction

We take the full spin hamiltonian to be:

$$H = H_M + H_Q \tag{1}$$

where H_M is the static magnetic interaction:

$$H_M = -\gamma h H_o I_z \tag{2}$$

with γ the nuclear gyromagnetic ratio, H_o the external magnetic field, taken to be along the z-axis, and I_z the z-component of nuclear spin. H_Q, the quadrupole hamiltonian, represents the interaction of the nuclear quadrupole moment with electric field gradients. It can be written:[4,5]

$$H_Q = \frac{eQ}{6I(2I-1)} \sum_{j,k} \frac{\partial^2 V}{\partial x_j \partial x_k} \times \left[3/2(I_j I_k + I_k I_j) - \delta_{jk} I(I+1)\right] \quad (3)$$

The indices j and k refer to axes x, y and z. Q is the quadrupole moment of the nucleus, e is the elemental charge, $\partial^2 V/\partial x_j \partial x_k$ represents a component of the electric field gradient tensor. To simplify the calculation, we limit ourselves to electric field gradients with cylindrical symmetry, and designate $eq = \partial^2 V \partial z'^2$, where z' is then the cylindrical axis of the field gradient. The quadrupole hamiltonian becomes:

$$H_Q = \frac{e^2 Qq}{4I(2I-1)} \Big\{ 1/2\ (3\cos^2\theta - 1)\left[3I_z^2 - I(I+1)\right] + 3/2\ \sin\theta\cos\theta\left[I_z(I^+ + I^-) + (I^+ + I^-)I_z\right] + 3/4\ \sin^2\theta\ (I^{+2} + I^{-2})\Big\} \quad (4)$$

where θ is the angle between the z and z' axes, and $I^{\pm}$ are the raising and lowering operators associated with the spin operator I, in the cartesian reference:[6]

$$I^{\pm} = I_x \pm i\, I_y \tag{5}$$

With the following definitions:

$$a = (3\cos^2\theta - 1) \tag{6a}$$

$$b = \sin\theta\ \cos\theta \tag{6b}$$

$$c = \sin^2\theta \tag{6c}$$

$$\alpha = \frac{e^2 Qq}{4I(2I-1)} \tag{6d}$$

and

$$\omega = -H_o \tag{6e}$$

the hamiltonian matrices for the spin systems I = 3/2 and I = 9/2 are as shown in Figures 3-3 and 3-4, respectively.

The energy levels of the system are found through second order perturbation theory:[7]

$$E_m^{(2)} = E_m^o + \langle m \mid H \mid m \rangle + \sum_j \frac{\left|\langle m \mid H \mid j \rangle\right|^2}{E_m^o - E_j^o} \tag{7}$$

$$H = \begin{bmatrix} \frac{3}{2}\omega + \frac{3}{2}\alpha a & 3\sqrt{3}\,\alpha b & \frac{3\sqrt{3}}{2}\alpha c & 0 \\ 3\sqrt{3}\,\alpha b & \frac{1}{2}\omega - \frac{3}{2}\alpha a & 0 & \frac{3\sqrt{3}}{2}\alpha c \\ \frac{3\sqrt{3}}{2}\alpha c & 0 & -\frac{1}{2}\omega - \frac{3}{2}\alpha a & -3\sqrt{3}\,\alpha b \\ 0 & \frac{3\sqrt{3}}{2}\alpha c & -3\sqrt{3}\,\alpha b & -\frac{3}{2}\omega + \frac{3}{2}\alpha b \end{bmatrix}$$

Figure 3-3. Hamiltonian Matrix for Spin I = 3/2 for Hamiltonian Defined by Eq. (1) Basis States are Taken to be $|I, m_I\rangle$, with Terms Defined in Eqs. (6a) to (6e)

$$H = \begin{bmatrix}
\frac{9}{2}\omega + 18\,\alpha a & 36\,\alpha b & 9\,\alpha c & 0 & 0 & 0 & 0 & 0 & 0 & 0 \\
36\,\alpha b & \frac{7}{2}\omega + 6\,\alpha a & 36\,\alpha b & 3\sqrt{21}\,\alpha c & 0 & 0 & 0 & 0 & 0 & 0 \\
9\,\alpha c & 36\,\alpha b & \frac{5}{2}\omega - 3\,\alpha a & 6\sqrt{21}\,\alpha b & \frac{9}{2}\sqrt{14}\,\alpha c & 0 & 0 & 0 & 0 & 0 \\
0 & 3\sqrt{21}\,\alpha c & 6\sqrt{21}\,\alpha b & \frac{3}{2}\omega - 9\,\alpha a & 6\sqrt{6}\,\alpha b & \frac{15}{2}\sqrt{6}\,\alpha c & 0 & 0 & 0 & 0 \\
0 & 0 & \frac{9}{2}\sqrt{14}\,\alpha c & 6\sqrt{6}\,\alpha b & \frac{1}{2}\omega - 12\,\alpha a & 0 & \frac{15}{2}\sqrt{6}\,\alpha c & 0 & 0 & 0 \\
0 & 0 & 0 & \frac{15}{2}\sqrt{6}\,\alpha c & 0 & -\frac{1}{2}\omega - 12\,\alpha a & -6\sqrt{6}\,\alpha b & \frac{9}{2}\sqrt{14}\,\alpha c & 0 & 0 \\
0 & 0 & 0 & 0 & \frac{15}{2}\sqrt{6}\,\alpha c & -6\sqrt{6}\,\alpha b & -\frac{3}{2}\omega - 9\,\alpha a & -6\sqrt{21}\,\alpha b & 3\sqrt{21}\,\alpha c & 0 \\
0 & 0 & 0 & 0 & 0 & \frac{9}{2}\sqrt{14}\,\alpha c & -6\sqrt{21}\,\alpha b & -\frac{5}{2}\omega - 3\,\alpha a & -36\,\alpha b & 9\,\alpha c \\
0 & 0 & 0 & 0 & 0 & 0 & 3\sqrt{21}\,\alpha c & -36\,\alpha b & -\frac{7}{2}\omega + 6\,\alpha a & -36\,\alpha b \\
0 & 0 & 0 & 0 & 0 & 0 & 0 & 9\,\alpha c & -36\,\alpha b & -\frac{9}{2}\omega + 18\,\alpha a
\end{bmatrix}$$

Figure 3-4. Hamiltonian Matrix for Spin I = 9/2 for Hamiltonian Defined by Eq. (1)
Basis States are Taken to be $|I, m_I\rangle$, with Terms Defined in Eqs. (6a) to (6e)

where we have taken the quadrupole interaction as a perturbation on the Zeeman term. From Eq. (7) with the aid of Figures 3-3 and 3-4 we can construct an energy level diagram, as shown in Figures 3-5 and 3-6 for the spin system I = 3/2 and I = 9/2, respectively.

3.3.2 Effects of Energy Level Shifts on the Precessing Spin System

We experimentally observe the spin de-phasing of a precessing nuclear sample by first creating a longitudinal nuclear polarization through spin exchange with optically pumped alkali vapor and then rotating the external magnetic field by 90 degrees to initiate precession of the nuclear spins. We equivalently describe this process in terms of the noble gas density matrix. We restrict ourselves here to nuclear spin I = 3/2; however, analogous equations can be written for the spin I = 9/2 case.

We assume that as a result of the alkali noble gas spin exchange interaction, the noble gas nucleus attains some low degree of polarization. In the low polarization limit, the density matrix for the noble gas system can be written:[8]

$$\rho = \begin{bmatrix} 1/4 + 3/2\zeta & 0 & 0 & 0 \\ 0 & 1/4 + 1/2\zeta & 0 & 0 \\ 0 & 0 & 1/4 - 1/2\zeta & 0 \\ 0 & 0 & 0 & 1/4 - 3/2\zeta \end{bmatrix} \qquad (8)$$

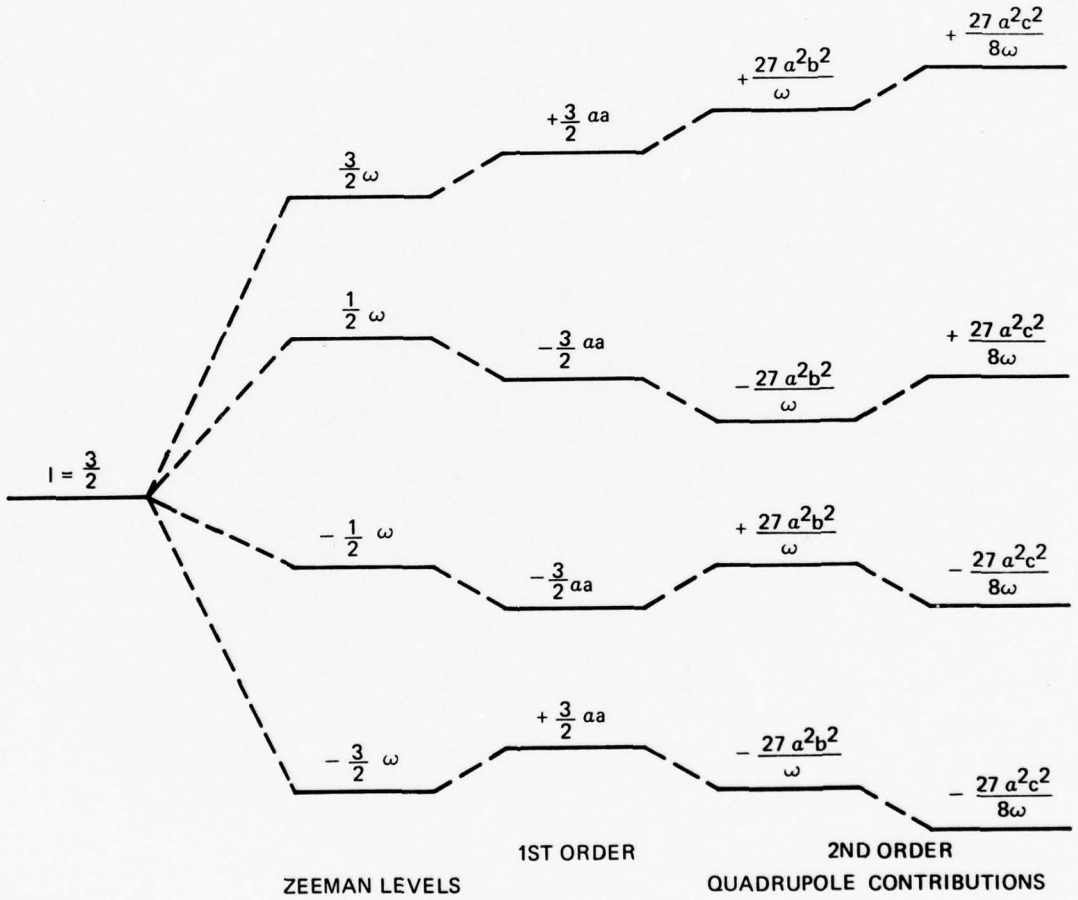

ENERGY LEVELS DEFINED BY EQ. (7) UNDER THE HAMILTONIAN DEFINED IN EQ. (1) WITH TERMS DEFINED IN EQS. (6a) TO (6e).

Figure 3-5. Energy Level Diagram I = 3/2

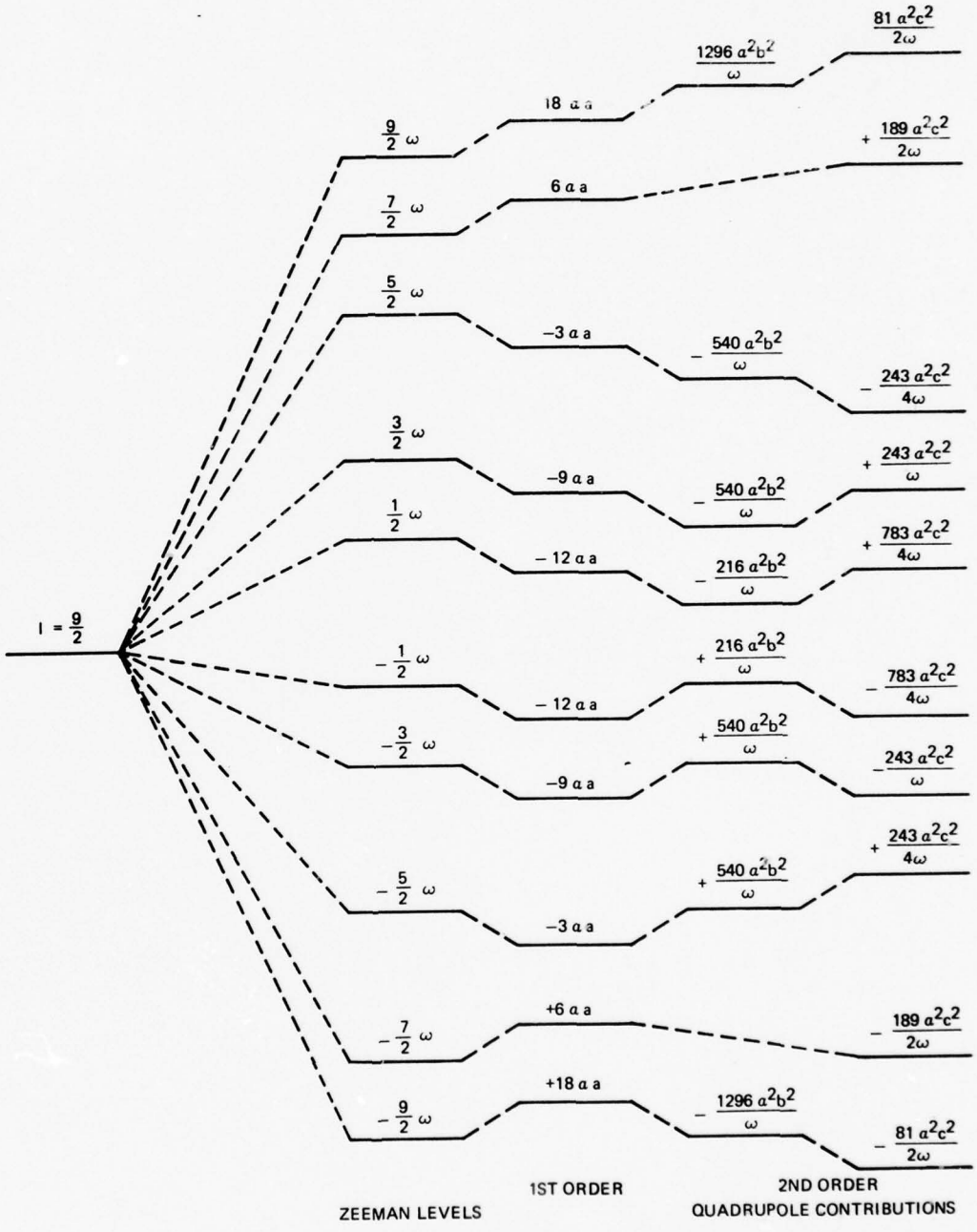

ENERGY LEVELS DEFINED BY EQ. (7) UNDER HAMILTONIAN DEFINED IN EQ. (1), WITH TERMS DEFINED IN EQS. (6a) TO (6e).

Figure 3-6. Energy Level Diagram I = 9/2

where ζ is a small number compared to unity. The factor, 1/4, is the equilibrium population density of each level. We can rewrite the initially prepared density matrix:

$$\rho = 1/4\,[I] + \zeta \begin{bmatrix} 3/2 & 0 & 0 & 0 \\ 0 & 1/2 & 0 & 0 \\ 0 & 0 & -1/2 & 0 \\ 0 & 0 & 0 & -3/2 \end{bmatrix} \tag{9}$$

where $[I]$ is the identity matrix.

Rotating the magnetic fields in the experimental apparatus is equivalent to a rotation of the density matrix, which is given by:

$$\rho' = D\rho\, D^{t} \tag{10}$$

where D is a Wigner D-matrix.[9] The D-matrix for a rotation of a spin 3/2 system about the y-axis through an angle ρ is shown in Figure 3-7. Substituting Eq. (9) into Eq. (10) and using Figure 3-7 we find the initial state of the rotated density matrix:

$$\rho'(0) = 1/4\,[I] + \zeta \begin{bmatrix} \cos\beta & -\sqrt{3}\sin\beta & 0 & 0 \\ -\sqrt{3}\sin\beta & \cos\beta & -2\sin\beta & 0 \\ 0 & -2\cos\beta & -2\cos\beta & -\sqrt{3}\sin\beta \\ 0 & 0 & 0 & -\cos\beta \end{bmatrix} \tag{11}$$

$$D^{3/2}(0,\beta,0) = \begin{bmatrix} \cos^3 \beta/2 & \sqrt{3}\cos^2 \beta/2 \sin \beta/2 & \sqrt{3}\cos \beta/2 \sin^2 \beta/2 & \sin^3 \beta/2 \\ -\sqrt{3}\cos^2 \beta/2 \sin \beta/2 & \cos^3 \beta/2 - 2\cos \beta/2 \sin^2 \beta/2 & -\sin^3 \beta/2 + 2\cos^2 \beta/2 \sin \beta/2 & \sqrt{3}\cos \beta/2 \sin^2 \beta/2 \\ \sqrt{3}\cos \beta/2 \sin^2 \beta/2 & \sin^3 \beta/2 - 2\cos^2 \beta/2 \sin \beta/2 & \cos^3 \beta/2 - 2\cos \beta/2 \sin^2 \beta/2 & \sqrt{3}\cos^2 \beta/2 \sin \beta/2 \\ -\sin^3 \beta/2 & \sqrt{3}\cos \beta/2 \sin^2 \beta/2 & -\sqrt{3}\cos^2 \beta/2 \sin \beta/2 & \cos^3 \beta/2 \end{bmatrix}$$

Figure 3-7. Wigner D-Matrix for Rotations About the Y-Axis of a Right-Handed Cartesian System, Through an Angle β

The precessional characteristics of the spin sample are described by the time evolution of the density matrix. The time dependence of the density matrix is given by:

$$\rho'(t) = U(t, 0)\ \rho'(0)\ U^{t}(t, 0) \tag{12}$$

where the evolution operator, U(t, 0) is defined through the differential equation:

$$\dot{U}(t, 0) = -i\ U(t, 0)\mathbf{H} \tag{13}$$

with the condition:

$$U(0, 0) = [I] \tag{14}$$

In solving Eq. (13), we have assumed that the quadrupolar contribution is small so that we may maintain the original eigenvectors of the magnetic hamiltonian while taking the eigenvalues through second order perturbation. The evolution operator becomes:

$$U(t, 0) = \begin{bmatrix} e^{-iEt_{3/2}} & 0 & 0 & 0 \\ 0 & e^{-iEt_{1/2}} & 0 & 0 \\ 0 & 0 & e^{-iEt_{-1/2}} & 0 \\ 0 & 0 & 0 & e^{-iEt_{-3/2}} \end{bmatrix} \tag{15}$$

The time dependence of the density matrix, using Eqs. (11), (12) and (15), is displayed in Figure 3-8.

$$\rho'(t) = \zeta$$

$$\begin{bmatrix}
\cos\beta & -\sqrt{3}\sin\beta\, e^{-i(E_{3/2} - E_{1/2})t} & 0 & 0 \\
-\sqrt{3}\sin\beta\, e^{i(E_{3/2} - E_{1/2})t} & \cos\beta & -2\sin\beta\, e^{-i(E_{1/2} - E_{-1/2})t} & 0 \\
0 & -2\sin\beta\, e^{i(E_{1/2} - E_{-1/2})t} & -\cos\beta & -\sqrt{3}\sin\beta\, e^{-i(E_{-1/2} - E_{-3/2})t} \\
0 & 0 & -\sqrt{3}\sin\beta\, e^{i(E_{-1/2} - E_{-3/2})t} & -\cos\beta
\end{bmatrix}$$

Figure 3-8. Time Dependence of the Noble Gas Density Matrix

The signal observed in our experiments corresponds to the expectation value of the x-component of the noble gas polarization, $\langle I_x \rangle$, defined to be:

$$\langle I_x \rangle = \mathrm{Tr}\left[I_x \ \rho' \right] \tag{16}$$

with the operator I_x for the spin 3/2 system written in matrix form as:

$$I_x = \frac{1}{2} \begin{bmatrix} 0 & \sqrt{3} & 0 & 0 \\ \sqrt{3} & 0 & 2 & 0 \\ 0 & 2 & 0 & \sqrt{3} \\ 0 & 0 & \sqrt{3} & 0 \end{bmatrix} \tag{17}$$

Thus our experiment is found to correspond to the following equation:

$$\langle I_x \rangle(t) = -\zeta \frac{\sin \beta}{2} \left\{ 3 \cos (E_{3/2} - E_{1/2})\, t + 4 \cos (E_{1/2} - E_{-1/2})t + 3 \cos (E_{-1/2} - E_{-3/2})t \right\} \tag{18}$$

For the case in which the quadrupole interaction is not present, the energy differences all become the same and Eq. (18) collapses to:

$$\langle I_x \rangle(t) = -5 \zeta \sin \beta \cos \omega t \tag{19}$$

which simply describes free precession of the spin system in a magnetic field.

Writing out the frequency terms in Eq. (18) we have:

$$E_{3/2} - E_{1/2} = \omega + 3\,\alpha a + \frac{54\,\alpha^2 b^2}{\omega} \qquad (20a)$$

$$E_{1/2} - E_{-1/2} = \omega - \frac{54\,\alpha^2 b^2}{\omega} + \frac{27\,\alpha^2 c^2}{4\omega} \qquad (20b)$$

$$E_{-1/2} - E_{-3/2} = \omega - 3\,\alpha a + \frac{54\,\alpha^2 b^2}{\omega} \qquad (20c)$$

noting that the terms a, b and c have angular dependence. From Eq. (18), we see that a quadrupole type interaction results in three precession frequencies for a spin 3/2 system. In general then, a spin system described by spin I will have 2I precession frequencies in the presence of a quadrupole type interaction. The different frequencies can be seen to be not only a function of the strength of the quadrupole interaction but also of the relative orientation of the electric field gradient with respect to the external magnetic field direction.

Examples of the precession signal described by Eq. (18) are displayed in Figures 3-9 and 3-10. Figure 3-9a is an example of the free precession signal in the absence of any quadrupolar interaction, presented for the purpose of comparing the effects of the presence of the quadrupolar interaction. The strength of the quadrupole interaction is the same in Figures 3-9b to

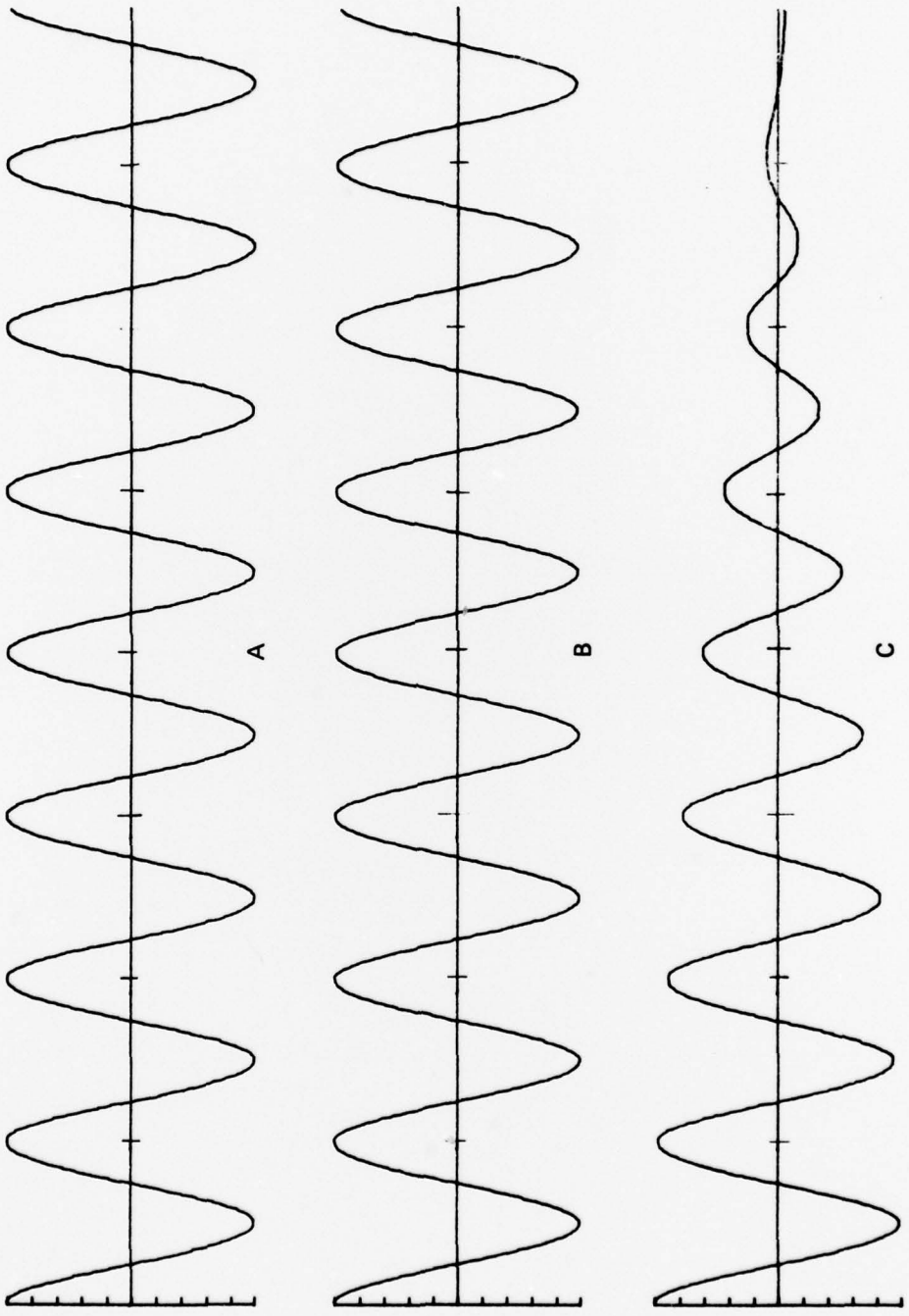

Figure 3-9. Free Precession Signal of a Spin 3/2 System in the Presence of a Quadrupolar Interaction

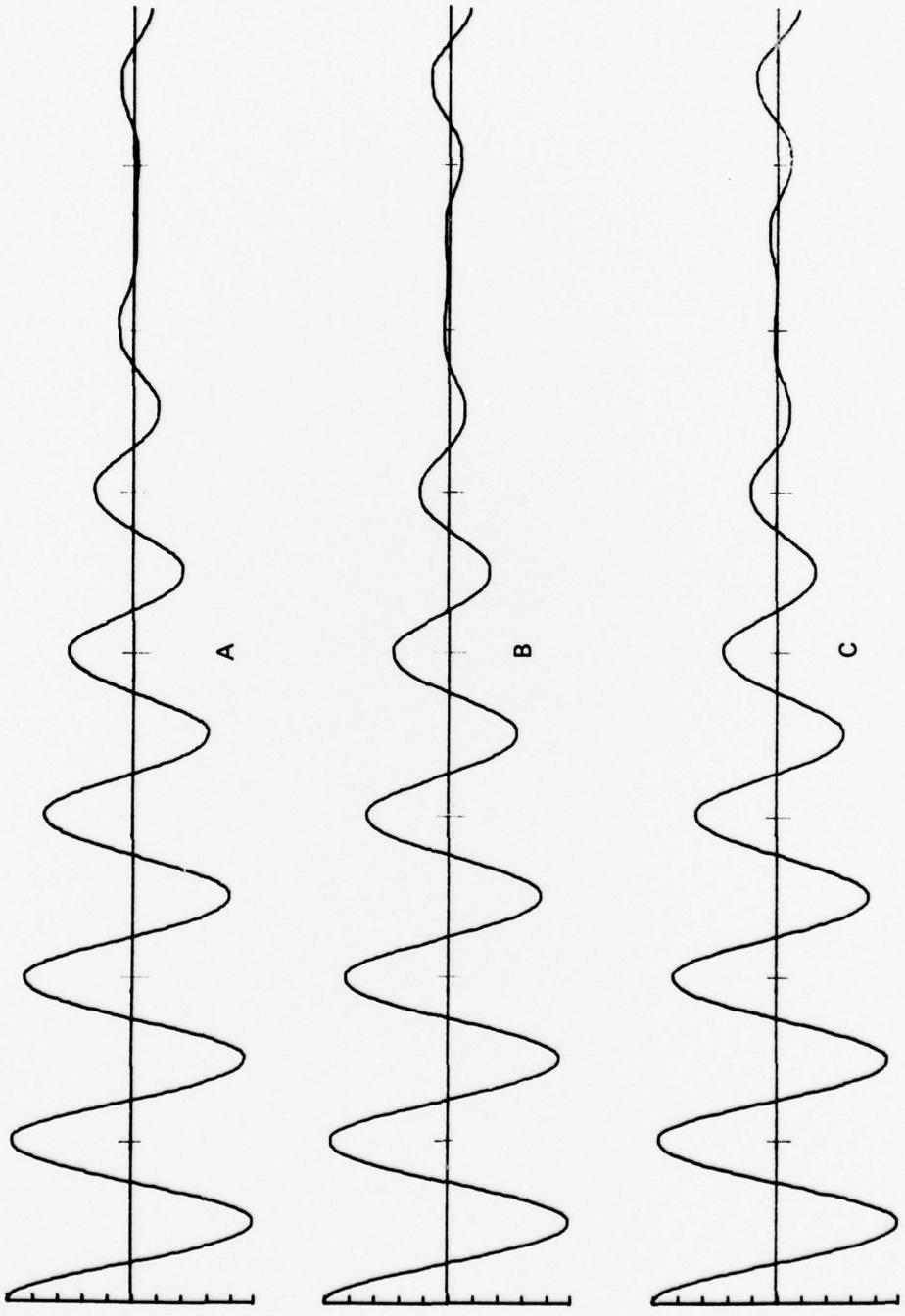

Figure 3-10. Free Precession Signal of a Spin 3/2 System in the Presence of a Quadrupolar Interaction

3-10C and was taken to be 2 percent of the magnetic interaction. The plot displays the effect of the angular orientation.

Figure 3-9b was attained by forcing the first order contribution of the quadrupolar interaction to zero. This is accomplished by setting the term $(3\cos^2\theta - 1)$ to zero. The angle θ is found to be approximately 55 degrees, which has previously been designated as the 'magic angle'.[1] Figure 3-9c corresponds to an angular orientation of 75 degrees, about 20 degrees off the magic angle; and Figures 3-10a, 3-10b and 3-10c represent orientations of 80, 85 and 90 degrees, respectively. The tick marks on all the plots designate the time position of the positive peaks of the free magnetic precession signal.

Various aspects of the Kr^{83} data can now be explained in terms of our model, albeit the model was derived for a spin 3/2 system:

a. There is an apparent decay of the precession signal as a function of angle. It is apparent in the sense that Eq. (18) describes three oscillatory signals which beat with one another. The beat envelope then is interpreted as a decay. If we were to extend the time axis on Figures 3-9c to 3-10c one would see the signal increase again in time. This phenomenon is not seen in the actual Kr data due to the presence of other decay processes which drive the signal amplitude to zero.

b. The beat envelope is not an exponential function. The Kr data is some combination of exponential decay due to 'real' decay processes modulated by the beat frequency. Near the magic angle, the signal is well described by an exponential function and quadrupolar effects are a minimum, while at angles more distant from the magic angle the decay signal develops a more non-exponential character.

c. Using the tick marks on the plots as a reference one can see that the precession frequency becomes shorter with time as a function of angle. Figures 3-10a through 3-10c show a phase reversal in the decay signal.

3.3.3 Origin of the Angular Effects

We noted earlier that the Kr decay data was influenced by the position of the excess Rb metal on the walls of the cell and that the Kr spin relaxation rate was a function of the cell size. We understand these facts to imply that the Kr experiences a quadrupole interaction in collisions with the cell walls.

It has been argued that in a collision of a noble gas atom with a cell wall, the atom is temporarily bound to the wall through a Van der Waals type interaction.[3] The depth of the well between the atom and a particular wall site is proportional to the surface adhesion energy. The electronic charge cloud of the

atom undergoes a distortion during the atom-wall interaction which results in an electric field gradient at the nucleus, proportional to the curvature of the potential well.

We can divide the binding sites on the cell walls into two distinct classes; one in which the noble gas atoms bind directly to the glass wall and the other in which the noble gas atoms bind to the layer of deposited Rb metal. One would expect that the adhesion energies between noble gas atoms and glass to be different from those of noble gas atoms and alkali metal. Since it is observed that the alkali metal does not uniformly distribute over the glass surface then it must be true that there is an angular distribution of adhesion sites on the cell wall. Notice that this argument does not depend on the strength of the binding energy of the noble gas atom glass sites compared to the noble gas atom alkali metal sites; only that the adhesion be different between the two classes of sites. In addition, the angular distribution of binding sites will be only weakly dependent on the macroscopic shape of the cell. The angular dependence observed in the Kr data results from the averaging over the binding sites with respect to the z-axis defined by the external magnetic field; as the cell is rotated, the averaging with respect to the space stationary z-axis changes and yields the observed angular effect. Redistributing the excess Rb metal on the cell wall changes the angular distribution of the binding sites and thus changes the angular effect at a particular cell orientation.

Wall collision effects on spin systems exhibit a strong dependence on the surface to volume ratio of the cell. This general feature has been observed in our experiments, which gives us confidence in our model of the Kr wall collisions.

3.3.4 Level Transition Effects

The true relaxation rate of a spin system through a quadrupole coupling of the nucleus with the electric field gradients which appear at the nucleus during the interaction of an atom on a wall has been worked out for Hg^{201} by Cohen-Tannoudji.[5] The time evolution of the nuclear density matrix is given by the formula:

$$\frac{d\rho}{dt} = -\int_0^\infty \overline{\left(H_Q^*(t), \left[H_Q(t-\tau), \rho(t)\right]\right)}\, d\tau \qquad (21)$$

which is second order in the quadrupole hamiltonian as compared to the pseudo-relaxation through level shifting which is first order in the interaction hamiltonian.

Eq. (21) also governs the longitudinal effects due to the quadrupole interaction. The degree of angular effect resulting from relaxation described by Eq. (21) would be readily apparent in the measured T_1 rate; however, no angular effects have been observed in the Kr T_1 measurements and thus we conclude that we

may average over all angles uniformly in the solution of Eq. (21) and thus directly apply Cohen-Tannoudji's results to the spin 3/2 system.

For isotropic orientations of the electric field gradient, Eq. (21) is shown to become:

$$\frac{d\rho}{dt} = -\,1/36 \sum_{r} J_r\left(A^r,\ \left[A^{-r},\ \rho(t)\right]\right) \tag{22}$$

where the index r runs from -2 to +2 and,

$$A^{\circ} = 3I_z^2 - I(I+1) \tag{23a}$$

$$A^{\pm 1} = \sqrt{6}/2\ (I_z\ I^{\pm} + I^{\pm}\ I_z) \tag{23b}$$

$$A^{\pm 2} = \sqrt{6}/2\ \left(I^{\pm}\right)^2 \tag{23c}$$

and

$$J_r = J_{-r} = \frac{36\pi}{5}\ \frac{\tau_s}{\tau_s + \tau_v}\left[\frac{e^2qQ}{I(2I-1)}\right]^2\ \frac{\tau_c}{1 + (r\omega\tau_c)^2} \tag{24}$$

For the magnetic fields present in our experiments:

$$(r\omega\tau_c)^2 \ll 1$$

and thus the quadrupole relaxation described by Eq. (21) is characterized by a single rate constant, J, in our experiments. From Eq. (13b) of Ref. 5, the decay of the transverse polarization can be shown to be given by the following formula:

$$\langle \dot{I}_x \rangle = -2 J \langle I_x \rangle \tag{25}$$

which is a simple exponential decay function. The transverse decay of a spin system due to a quadrupole interaction is described by the function represented in Eq. (18) multiplied by an exponential decay.

3.4 SUMMARY

We have experimentally measured the pumping and decay characteristics of Kr^{83} as a function of the orientation of the Kr cell in our experimental apparatus. We have qualitatively explained our observations based on a model in which the nuclear spin is 3/2. In addition, we have written the analogous equations for spin 9/2; however, due to the complexity of the spin 9/2 system, we have not been able to stabilize our computer codes enough to give us reliable Least Squares fits to our Kr data based on our model. We do not feel that this is due to any inherent difficulty in our model.

3.5 CONSIDERATIONS FOR FUTURE WORK

We plan to measure the decay characteristics of Xe^{131} in a manner similar to that done for Kr^{83}. Due to the inherently simpler properties of the spin 3/2 system as compared to that of the spin 9/2 system, we feel that we will be able to perform parametric fits to the Xe^{131} data and realize a quantitative verification of our relaxation model.

3.6 BIBLIOGRAPHY FOR SECTION III

1. D.S. Bayley, I.A. Greenwood and J.H. Simpson, "Noise Sources in NMR Oscillators and Relaxation Phenomena in Optically Pumped Mercury Isotopes," Final Scientific Report, AFOSR, 1976 (unpublished).
2. J.H. Simpson, Bull. Amer. Phys. Soc. 23, 394 (1978).
3. W. Happer, private communication, 1978.
4. A. Abragam, "The Principle of Nuclear Magnetism," Oxford at the Clarendon Press, 1961, Ch. 8.
5. C. Cohen-Tannoudji, J. de Phys. 24, 653 (1963).
6. L.I. Schiff, "Quantum Mechanics," McGraw-Hill Book Co., New York, 1968, p. 200.
7. ibid, p. 247.
8. L.W. Anderson and A.T. Ramsey, Phys. Rev. 124, 1862 (1961).
9. A.R. Edmonds, "Angular Momentum in Quantum Mechanics," Princeton University Press, 1957, Ch. 4.